nuclear fusion
IAEA

PAPER • OPEN ACCESS

Thermal management and net-power evaluation of the ST-E1 fusion power plant

To cite this article: Mohamed Khalid Elsharif Mohamed *et al* 2026 *Nucl. Fusion* **66** 086005

View the article online for updates and enhancements.

You may also like

- Fusion pilot plant performance and the role of a sustained high power density tokamak
J.E. Menard, B.A. Grierson, T. Brown et al.
- Power plant conceptual studies in Europe
D. Maisonnier, D. Campbell, I. Cook et al.
- The new layout and regulation of the 'pulsating' power conversion system of EU DEMO WCLL for an effective and safe control of pulse-dwell transitions and increase in plant efficiency
L. Barucca, A. D'Alessandro, A. Burlando et al.

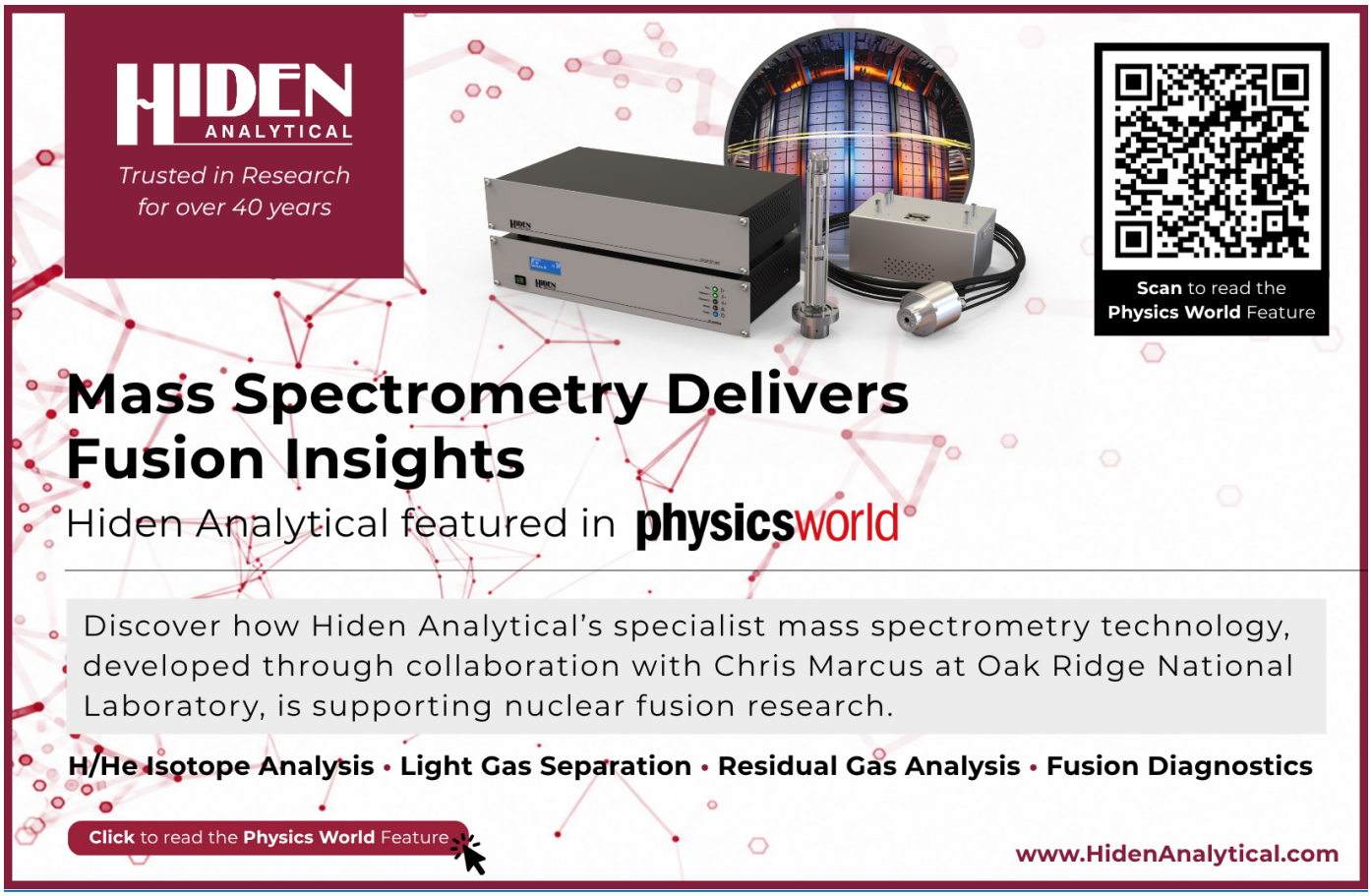

This content was downloaded from IP address 130.51.23.114 on 03/11/2026 at 03:04

OPEN ACCESS
IOP Publishing | International Atomic Energy Agency
Nuclear Fusion
Nucl. Fusion **66** (2026) 086005 (25pp)
https://doi.org/10.1088/1741-4326/ae5546

Thermal management and net-power evaluation of the ST-E1 fusion power plant

Mohamed Khalid Elsharif Mohamed*, Alasdair Burchill, Liviu Maatescu, Emre Yildirim, Jonathan Naish, Matthew Robinson, Vandeep Godhani, Samara Levine, Sandeep Irukuvarghula, Chris Wilson, Ivan Krastev, Robin Kamenicky and Abhishek Kumar

Tokamak Energy Ltd, Milton Park, Oxfordshire, United Kingdom of Great Britain and Northern Ireland

E-mail: mohamed.mohamed@tokamakenergy.com

Received 18 December 2025, revised 10 March 2026
Accepted for publication 20 March 2026
Published 10 July 2026

Abstract

A comprehensive analysis of the thermal management and net-power performance is presented for the ST-E1 low aspect ratio tokamak fusion power plant. The study addresses the critical interplay between coolant system design, power cycle integration, and electrical loads, which significantly influence net-power projections and overall plant viability. Specifically, it quantifies the impact of coolant loop design, pressure drops, pumping power, and thermal storage on plant efficiency, and examines the conditions required to achieve the pilot-phase net power target of 300–500 MWe. The findings provide insight into the system-level trade-offs that govern fusion plant viability and inform pathways toward improved net-power performance.

Keywords: tokamak, fusion power plant, thermal management, power generation

(Some figures may appear in colour only in the online journal)

1. Introduction

ST-E1 is a modular, upgradable fusion power plant, based on a low aspect ratio tokamak configuration with a 5 m major radius and an on-plasma toroidal field (TF) of 5.25 T [1]. With an initial pilot phase seeking to generate 300–500 MWe (Megawatt electric) and an uprating to produce 800 MWe in the commercial phase. This utility, at full power-plant scale, must balance the recirculating power needed for the reactor and its auxiliary systems while controlling thermal loads on plasma-facing components, the breeder blanket, and shielding structures. ST-E1 intends to leverage steady-state operating design points, with the bulk of the pilot phase allowing for demonstration of key technologies to de-risk the uprated phase. The thermal and electrical analyses presented in this paper are based on the Reference Design Point (RDP) of ST-E1, as defined in the overview of this focused collection [1]. The RDP corresponds to a fusion power of 1573 MW_{fus} (Megawatt fusion) plasma in the pilot phase, with the reference ramp-up scenario for the electrical systems adopted from a representative ramp-up in [2]. This is the total power generated directly by the fusion reactions occurring inside the plasma. These define the neutronic and thermal loadings of the key components assessed herein representing the power exported from the device; while the RDP gives the steady loads, combined with the ramp-up case to represent the power draw from the plant.

Although steady-state operation remains the ultimate objective, the practical challenges associated with continuous

* Author to whom any correspondence should be addressed.

Original content from this work may be used under the terms of the Creative Commons Attribution 4.0 licence. Any further distribution of this work must maintain attribution to the author(s) and the title of the work, journal citation and DOI.

 © 2026 The Author(s). Published by IOP Publishing Ltd on behalf of the IAEA

24/7 operation persist [3]. Achieving a positive net power balance therefore depends on several interrelated factors over the reactor duty cycle [4]. These include, first, the duration of the flattop phase, which may be limited by impurity accumulation and other plasma phenomena [5]. Secondly, the allowable temperature range for constituent materials during operation, which can dictate the inlet and outlet temperatures for components as well as their cooling requirements. Third, the magnitude of recirculating power during the pulse, including the heating, current drive, and pumping loads of the thermal systems and overhead of the plant [4, 6]. And finally, the energy and time required for ramp-up/down and the dwell period between pulses, during which auxiliary systems continue to draw power despite the absence of fusion energy production. Collectively, these elements govern the average net electrical output and underscore the need for integrated optimisation of plasma performance and plant-level energy flows.

From these considerations, several guiding principles emerge. First, maximising the fusion gain (Q) and leveraging high bootstrap current are essential to reduce external heating and current-drive power [3]. Second, minimising ramp-up and ramp-down durations, and the associated energy penalties, can significantly improve the plant's net-power performance. Third, extending the flattop period increases the plant's capacity factor, enhancing overall energy yield. Finally, reducing parasitic loads from plant overheads, such as gas-compression and cryogenic systems power, is critical to achieving a favourable net power balance.

Steady-state plasma operation reduces cyclic fatigue, enabling higher availability, a key factor in plant economic viability. Due to the need to drive the plasma current non-inductively, efficient steady-state operation requires operating with high bootstrap current fractions to minimise the need for external current drive. The spherical tokamak and the advanced tokamak are the most promising steady-state concepts and share many attractive features [7].

This paper presents an integrated, plant-level assessment of ST-E1's thermal management and net-power performance that couples electrical load characterisation and distribution system modelling with detailed thermo-hydraulic analysis and process simulation. Section 2 presents the architecture of the plant's electrical system, categorises its loads, models the steady-state and pulsed networks, and incorporates converter and storage strategies that stabilise power quality and grid exchange. In section 3, heat extraction and power conversion from the breeder blanket, divertor, and Centre Column Shield (CCS) is evaluated, enabling a comparison of two thermal-management architectures: the Independent Helium Loops (IHLs) and the Coupled Helium Loops (CHLs) configurations, driven by two alternative divertor technologies. Building upon these results, section 4 carries out an integrated net-power assessment that consolidates and reconciles the findings from sections 2 and 3. The findings provide insight into the system-level trade-offs that govern fusion plant viability and inform pathways toward improved thermal integration and power-cycle optimisation.

2. Power in

To assess the net-power performance of the ST-E1 fusion power plant and to inform the design of the plant's electrical system, the recirculating electrical power profile is first determined. This is achieved by performing a characterisation and classification of the plant's electrical loads set out in the RDP [1]. The resulting load characterisation is then used as input for the preliminary design of the internal electrical distribution system. Based on this design, the main electrical components are sized and subsequently implemented in a PSCAD model [8].

2.1. The electrical power system of ST-E1

The Electrical Power Distribution and Storage System (EPDS) of ST-E1 provides the interface between the electrical grid, and all plant electrical loads. It transforms power between transmission and distribution voltage levels and distributes it to all loads, including the short-duration peak demands of pulsed magnet power supplies, while protecting personnel, plant equipment, maintaining voltage, an improved power factor (PF) and power quality, and providing a minimum security of supply for safety-related and asset protection-critical systems.

In common with related projects, for example ITER [9] and DEMO [4], the electrical power system design of ST-E1 is broadly divided into the Steady-State Electrical Network (SSEN) for continuous loads, plus the unit network associated with the generator connection and the Pulsed Power Electrical Network (PPEN) for pulsed loads, with the segregation of these networks required to satisfy the requirements of minimum power quality, security of supply, and redundancy.

The SSEN supplies loads with continuous or quasi-continuous demand, such that their demand is present outside of plasma pulses, at least while the plant is in an operationally-ready state, and their demand does not vary significantly during plasma pulses (e.g. pumping for primary cooling, cryogenic plant, and cooling water plant). The SSEN also supplies the balance of plant, including site safety systems, lighting, IT, HVAC, and other hotel loads. The SSEN is required to meet minimum standards of power quality by design, including voltage regulation, total harmonic distortion (THD) and flicker. This is facilitated by electrical separation from large-scale pulsed loads. The additional requirements of high availability and security of supply by Safety Critical (SC) and Investment Protection (IP) loads will be satisfied by a combination of diesel generators (DGs) and uninterruptible power supplies (UPSs), as required.

The PPEN supplies loads with pulsed demand which is only present during one or more phases of plasma pulses. Examples of such loads include the poloidal field (PF) and central solenoid (CS) field coils of the tokamak, and the plasma heating and current drive (HCD) systems. Such pulsed demand is inevitably detrimental to power quality on the PPEN, however, it is assumed that a lower standard of power quality may be tolerated. In addition to pulsed loads, the PPEN accommodates

electrical energy storage, providing the facility to augment power imported from a grid connection during periods of pulsed demand, thereby smoothing the power import profile and limiting the maximum magnitude of import to meet a grid connection agreement. Electrical energy storage also fulfils a regenerative function, buffering energy which is extracted from the PF and CS coils.

When the plant is generating electrical power, in continuous or long-pulse operation, a fraction of the generated power is used to serve demand on the steady-state and pulsed networks, with the balance being exported to the grid.

2.2. Steady state loads

An initial load survey of all major plan systems (using the logical Plant Breakdown Structure organisation of ST-E1 as a starting point) is carried out, by classifying and characterizing all known electrical loads at this stage of the plant's design. The listing in table 1 contains only active subsystems, that require an electrical energy supply. The first evaluation of the electrical power demand is using information available from an initial forecast by system owners or available literature (where system design was still preliminary) [10–12]. For each main system, a description is provided on how the electrical supply is facilitated, with a reference to the power distribution preliminary architecture further discussed in section 2.4.

The size of the main loads was estimated based on existing similar industrial electrical infrastructure, in terms of apparent power, and their peak values are reported in table 1. For equipment sized as part of a different subsystem design (e.g. compression powers reported for the tokamak systems), initially reported as active power demands, a typical industrial plant PF target of 0.85 was considered [12, 13], with room for later improvement if different pumping technologies are assumed (e.g. High Voltage (HV) frequency converters) or if local reactive power compensation is envisaged on dedicated buses.

Another aspect of the load survey and size estimation process is that certain portions of the electrical demand, although identified, are not actually included. This is either because the associated loads are very small compared with the total demand, or because this demand is unlikely to occur at the same time as the pulsed operation. In addition, some electrical loads are currently counted within other individual systems rather than being grouped into a single larger, stand-alone system. This situation may change as the PBS is further refined and made more detailed (for example, some local control systems are still treated separately, and remote handling is still included under the Hot Cell, etc).

For several subsystems, the electrical demand depends strongly on which of the two ST-E1 thermal management process architectures (IHL or CHL) is adopted; consequently, two distinct demand values are provided. Also, the load demand assumptions are valid only for the pulse/flattop operation period, and it is acknowledged that during the dwell period this value is lower.

The Tokamak Systems electrical loads relate to the primary heat transport circuit, in particular the primary helium coolant loops for the two thermal management architectures. For this analysis, helium compressor power is treated as a lumped value for each loop; the final number of compressors will depend on the optimised number of independent circuits.

Compressor electrical power for the full compression stage, from the thermo-hydraulic analyses (more details are provided in section 3), is 34 MW / 27.1 MW (CCS), 38.8 MW / 265 MW (Divertor), and 141 MW / 63.2 MW (Breeder Blanket) for the two divertor configurations. The breeder blanket figure includes 4.44 MW for lithium pumping power, driven by the lithium pumps in the primary lithium loop. Other auxiliary loads in the tokamak primary heat transport systems are excluded from this forecast.

These loads are assumed to be supplied from the 13.8 kV busbars of the Steady State distribution network, arranged to give uniform loading on five busbars for the HP-PFU configuration or nine for the Helium-cooled Modular Jet (HEMJ) configuration. Their high power demand and the intermittent heat transfer from the fusion island (during dwell time) make them good candidates for future power reduction via variable-speed technologies. The operating regime is primarily constrained by allowable compressor speed variation rates [14]. The main Hot Cell facility electrical infrastructure supports transfer, remote handling operations and radwaste management processes, with their associated electrical loads such as cranes, transfer tools, various robotic manipulators and radwaste storage/treatment/export [15]. While the former groups account for some degree of loads diversity, the latter comprises of larger continuous running systems such as Local Air Coolers (LACs) for detritiation systems and HVAC. In an initial assumption, the electrical power demand of this system is about 3 MVA.

The Fuel Processing System is an auxiliary system for cleaning generated and unburnt fuel species. Its main electrical loads are water, gas and air detritiation equipment, cryogenic separation columns, electrolysers and small auxiliary loads, totalling 3.5 MVA with a PF of 0.95. It also includes vacuum systems for the vacuum vessel (cryopumps, roughing pumps and service pumps) with 1.45 MVA installed power.

The matter injection subsystem (hydrogen isotope fuelling, plasma control gases and vessel conditioning) mainly uses cryo-compressors and low-power local control systems, totalling 1.6 MVA. Together with support systems (mainly LACs and a dedicated HVAC system, about 0.42 MVA), the total installed power is 7 MVA.

As most equipment is low power, the plant will be supplied by three dedicated LV substations, distributed over at least two main supergrid Steady State network connections. Due to possible nuclear safety classification linked to tritium inventory, the electrical distribution design should allow for enhanced supply security (redundant and segregated supplies, backup supplies).

The Control Systems and Infrastructure group is a placeholder for electrical loads associated with plant-wide control systems, aligned with standards for power generation and

Table 1. Summary of ST-E1 main load groups and electrical power demand.

System	Main subsystem	Power [MVA] (IHL / CHL)
Tokamak Systems		
	Magnet Assemblies (passive)	0.00
	HCD Hardware (passive)	0.00
	Centre Column Shielding	37.78 / 31.15
	Divertors	44.09 / 301.14
	Breeder blanket	161.11 / 77.09
	Vacuum vessel	2.00
	Matter injection	0.10
	Cryostat	0.10
	Plasma diagnostics	1.20
Reactor Hall Bioshield		0.00
Hot Cell		2.97
Fuel Processing Systems		
	Matter injection	1.60
	Exhaust processing	0.08
	Isotope rebalancing & Separation	1.60
	Tritium exhaust	0.01
	Gas detritiation (+ Air detritiation system)	0.09
	Water detritiation	0.04
	Isotope separation	1.60
	Fuel storage	0.10
	Other systems	0.42
	Plasma vacuum	1.45
Control Systems and Infrastructure		0.55
Electrical Systems		
	TF power supply	0.60
	Power supplies auxiliaries	3.65
	Backup power auxiliaries	0.10
	Power distribution—HV substations	0.97
	Power distribution—Generator TX	0.15
	Main generator	2.28
	Electrical power storage	0.41
Thermal Systems		
	High temperature heat circuit	2.35
	Cryogenic supply	10.75
	Power generation	40.04
	Low grade heat rejection	12.92
Site Utilities		
	HVAC	2.45
	Lighting	0.50
	Gases	0.02

chemical process plants. It includes a Distributed Control System (DCS) as the central plant orchestrator, providing human–machine interfaces (HMIs) for operations and acting as a process historian to store and retrieve selected plant-wide variables over short-, medium-, and long-term periods for analysis and troubleshooting. It also hosts the Radiological Surveillance System (RSS), which collects real-time and survey-based radiological data. For conventional heat exchange and energy production systems, control will be implemented directly by the DCS. For the Balance of Plant and plasma control, bespoke controllers will manage inter-system logic and overall plant integration. The total estimated demand

for this system is 0.55 MVA, highly dependent on practical hardware choices for the Plant Control and Monitoring System. For supply security, these loads will be fed from the unit's main bus, backed by local diesel generation and partial UPS support.

The Electrical Systems category covers all auxiliary electrical demand for power distribution. Main loads are the Electrical Generator (hydrogen and water cooling, excitation) and HV distribution transformer cooling, assumed ONAF type. Switchgear and transformer control supplies are included in this category. Except for the generator excitation transformer, which usually taps off at the generator output at the same voltage level, all other loads are LV and grouped, for initial design, under two LV distribution substations. A supply is also assumed for Energy Storage System environmental conditioning to maintain proper battery/ultracapacitor climate control. The power supply auxiliary subsystem includes control systems, air cooling of magnet power supply transformers, and gyrotron auxiliary power supplies (heater, anode, body, magnet). Most have constant or slowly varying profiles; the time-varying loads are small enough that their impact on SSEN power quality is negligible.

The TF magnet operates at nearly constant current and uses relatively low-power converters, therefore its power supply can be fed from the Steady State network without significantly affecting other loads; its design can readily include PF correction. For a TF design current of 50 kA, the supply has a maximum ramp rate of 1 A s^{-1} and a maximum voltage of 56 V, giving a peak power of 2.8 MW (or 1.4 MW with constant-power ramp-up). Once the TF current reaches its steady-state setpoint, the supply output is reduced, limiting the required electrical power to about 0.6 MVA including auxiliaries (e.g. local cooling). Since current ramp-up occurs before operation and plasma breakdown, and does not overlap with the high-power-demand period, this lower value is used in the power figures. As per power supply to PF/CS coil connection, it is assumed that superconducting busbars are employed for power supply to TF coil connection on ST-E1.

The Cryogenic System, part of the Thermal Systems group in the electrical classification, assumes modular turbo Brayton units as plant cryogenic sources. Its main electrical loads are centrifugal compressors, cryofans, and compressors for a local chilled water system. Each of the first two loads belongs to a stand-alone cryogenic module and requires a single LV supply, served by two dedicated LV substations. The chilled water system is dedicated to the cryoplant, with some components fed from another dedicated LV substation and the main compressors supplied from high-voltage intermediate buses, likely at 6.9 kV due to the size of typical HV chilled water compressors. The total electrical demand of the cryogenic system is 10.75 MVA. Its role is to provide cooling for the magnet system. Other systems with cryogenic needs (e.g. Electron Cyclotron Resonance Heating (ECRH) superconducting magnets, vacuum cryopumps, matter injection) have their demands included in their own electrical figures, assuming independent local refrigeration.

Table 2. Summary of ST-E1 electrical total power demand (steady-state).

System	Peak power [MVA] (IHL / CHL)
Tokamak Systems	246.28 / 412.67
Reactor Hall Bioshield	0.00
Hot Cell	2.97
Fuel Processing Systems	7.00
Control Systems and Infrastructure	0.55
Electrical Systems	8.16
Thermal Systems	66.06
Site Utilities	2.97
Total	**333.98 / 500.37**

The Power Generation system, part of the Thermal Systems group, includes the majority of loads associated with the electrical generation plant. These loads are tied to the thermal cycle, which in ST-E1 uses an advanced supercritical Rankine steam cycle described in the Power Out section. The cycle's main components are the steam generator and auxiliary steam systems with superheater and reheater stages, three steam turbines (high-, intermediate-, and low-pressure), condenser, regenerative condensate heating stages, deaerator and feedwater pumps. Thermo-hydraulic analysis indicates 1.2 MW of condensate pumping power and 31.7 MW of feedwater pumping power, with a typical PF of 0.85. Other auxiliary steam-cycle components, plus cooling-water and chilled-water plants in the final heat sink cooling system, add 12.92 MVA. Various pumps supply the required pumping power, with the largest using 6.3 MVA motors from the 13.8 kV main unit bus. These are the largest plant loads requiring direct start, so refinement of the unit bus architecture and upstream transformers will focus on meeting allowable nodal voltage limits in steady state and during startup transients.

The main electrical part of the Site Utilities is composed of the HVAC and lightning systems, and they all amount to about 3 MVA of electrical power.

The conclusion of the power forecasting exercise, for the Steady State loads of the plant, can be summarised in the following table 2. In the total balance of plant these powers are referenced as plant loads recirculating powers.

2.3. Pulsed power loads

2.3.1. Magnet power supply system. The superconducting TF magnets of ST-E1 are intended to be charged prior to plasma pulse operations, and then held at-field for the duration of an operational campaign period—in the order of weeks or months. The rate of charging may therefore be slow, with a maximum anticipated power demand of approximately 600 kVA. Since this load is comparatively insignificant, and charging of the TF coil will not be concurrent with plasma operations, the demand is considered within the steady-state load subsection.

The PF and CS coils are used to shape and control the position of the plasma, as well as to induce plasma current. The power supplies of these coils are required to drive rapidly changing coil currents in four-quadrant operation. The conventional technology choice for such converters has been thyristor-based 12-pulse converters [16–18]. However, this converter technology has the disadvantages of limited dynamic performance, very high reactive power demand, and significant harmonic disturbance. The proposed architecture for the PF and CS coil converters of ST-E1 is a full-bridge Multilevel Modular Converter (MMC) topology. The ongoing design and development of this power supply approach is being informed by requirements and benefits which include:

- **Low reactive power demand and harmonic disturbance**: Converters of this type may be operated at close to unity PF, and may be designed to produce very little harmonic distortion, minimising the requirements for PF correction and harmonic filtering.
- **Intrinsically modular architecture**: The modular nature of the topology facilitates a modular power supply architecture, in which power supplies are assembled from standardised 'building blocks', and may be operated de-rated, with constituent modules bypassed, if required.
- **Standardisation of components**: The modular architecture de-risks procurement, since design decisions such as rating may be deferred, with power supplies scaled with the addition or removal of modules over the course of plant lifetime. The use of common and standardised components and assemblies also provides the advantages of a less constrained supply chain, and a simplified, common spares inventory for converters.

Whilst recognising that PF/CS coil converters using switching technology have not yet been widely adopted and validated in the fusion industry, it is considered that these benefits justify the practical development and implementation challenges.

Switching network units (SNUs) have been specified on other tokamak projects of comparable scale to ST-E1 in order to achieve the very high current derivative required to initiate plasma breakdown [9, 17, 19]. Since the time-step of the simulated CS coil currents available at the pre-conceptual design stage was too coarse to capture the sub-millisecond breakdown dynamics that would dictate SNU requirements, their use is not considered at this stage. It is acknowledged that a more detailed study of the plasma breakdown phase would be required in subsequent design stages to inform SNU requirements.

Superconducting PF/CS busbars are the proposed design choice for ST-E1, since the losses in room-temperature busbars over the distances anticipated between the coil power supplies and the tokamak amount to the multi-MW scale. Further advantages include the greater scope for concentric conductor arrangements to cancel stray fields and reduce electromagnetic (EM) loading on supports, and the avoidance of multiple current leads in close proximity to the cryostat of the tokamak, where space is at a premium. It is therefore assumed that superconducting busbars are employed for power supply to PF/CS coil connection on ST-E1, whilst recognising the cooling requirements and other engineering challenges. The design and development of high-current superconducting busbars is the subject of ongoing work.

The PF/CS power supplies are intended to provide the facility for a controlled ramp-down of coil current, for the purpose of coil protection in the event of a fault or quench. Beyond this, the requirements for coil protection plant, such as fast discharge units (FDUs), are not considered further at this design stage within+ the context of electrical power systems, but will be informed by coil protection requirements as these are understood more fully.

2.3.2. Plasma HCD power systems. Radio frequency (RF) HCD is to be achieved on ST-E1 using ECRH with gyrotrons as the RF source. Of the three principal power supplies required to drive gyrotron tubes: cathode, anode and body, the cathode power supply strongly dominates the total electrical power load, with a demand orders of magnitude higher than the other two power supplies. Accordingly, the demands of the gyrotron anode and body power supplies were not considered further at this design stage.

The efficiency of current gyrotron technology, from wall-plug electrical power to RF output power, is approximately 50% in advanced prototypes. Hence, this figure is considered an expected target efficiency, recognising that further RF losses will occur in waveguides and antennas, and from sub-optimal plasma coupling [20–23]. Accordingly, the electrical demand of the gyrotrons, negating the rejected heat that is considered under steady-state demand, may be approximated as follows:

$$P_{\mathrm{RF}}(t) = \eta P_{\mathrm{GRID}}(t) = \eta S_{\mathrm{GRID}}(t)\cos\varphi \tag{1}$$

$$S_{\mathrm{GRID}}(t) = \frac{P_{\mathrm{GRID}}(t)}{\cos\varphi} = \frac{P_{\mathrm{RF}}(t)}{\eta\cos\varphi} \tag{2}$$

where P_{RF} is the RF power output, P_{GRID} is the electrical real power input, S_{GRID} is the electrical apparent power input, η is the overall efficiency, and $\cos\varphi$ is the PF. A PF of 0.95 is assumed [20].

Current drive and RF heating power during the flattop phase are included based on preliminary power assessments. Nevertheless, a full transient evaluation of the heating and current ramp-up stages has not yet been performed at this point in the design.

2.3.3. Electrical energy storage. Electrical energy storage is utilised for three principal functions:

- To reduce peak pulsed power exchange with the grid
- To reduce the rate-of-change of grid power exchange
- To regeneratively buffer reverse power flow during coil discharge

These roles are most significant during plasma start-up and ramp-down. Electrical energy storage will not be used to buffer discontinuous electricity generation as a result of pulsed machine operation. Rather, thermal buffering within the cooling cycles will permit continuous generation.

It has been demonstrated by modelling that electrical energy storage may be distributed within a PF/CS power supply fleet, in order to fulfil the functions presented above. The coil currents and voltages, in addition to ECRH power represent a representative ST-E1 scenario, produced by the SCOPE (Simple Coil Optimiser for Physics and Engineering) optimiser in [2]. SCOPE is an in-house tool that designs PF and CS coils to satisfy physics requirements while ensuring operation remains within the limits of high-temperature superconductor (HTS) magnets. The proposed storage technology to be employed is the electric double layer capacitor (EDLC), used to increase DC-bus energy storage capacity within the power convertors. The peak instantaneous aggregated active power of all PF/CS coils, 1–20, in the reference scenario is approximately 2200 MW. This was considered in the context of illustrative grid connection constraints, based on those of the 400 kV transmission network connection of UKAEA's JET [24]. A peak grid connection active power for the pulsed-power network of $+/-500$ MW was therefore imposed, with a maximum rate-of-change of grid active power of 50 MW s^{-1}, for the purposes of these optimisations. This included the demand of HCD. Whilst it was assumed that the grid connection could accommodate bi-directional power flow within the specified limits, transmission system operators may not accept large oscillatory power exchanges, and so additional electrical energy storage or dump loads may be required to comply with grid connection constraints at subsequent design stages. A PF/CS converter front-end (grid-side) active power limit of $+/-500$ MW was also imposed. Linear optimisation was employed, using the Python SciPy library, in order to determine the optimal allocation of distributed energy storage capacity across PF/CS coil converters, in order to meet the imposed grid connection power exchange limits, whilst minimising the total stored energy capacity. The optimisation was formulated with the following lexicographic objectives:

- Minimise total required energy storage capacity
- Minimise circulating power between converters
- Maximise pre-charging during the period prior to plasma start-up

It was found that, for the reference scenario, with a 300 s pre-charge period, prior to plasma start-up at $t = 0$, during which pre-charging of both PF/CS coils and energy storage is permitted, the constraints could be met with a total electrical energy storage capacity of approximately 1.52 MWh. The distribution of this capacity across a subset of the PF/CS converters, is shown in figure 1.

The state of charge (SoC) of the energy storage added to the subset of converters, and dictated by optimal dispatch in the reference case, is presented in figure 2.

The active power exchange at the front-end (grid-side) of all converters, limited to within ± 500 MW by the additional energy storage distributed across the converters as required, is presented in figure 3.

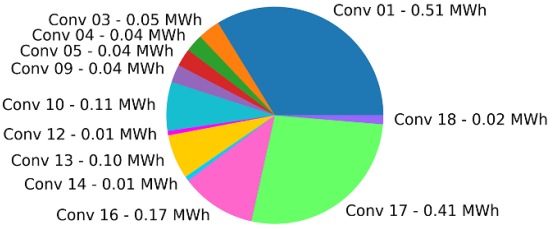

Figure 1. Additional supercapacitor energy storage added to a subset of converters following optimisation based on reference case.

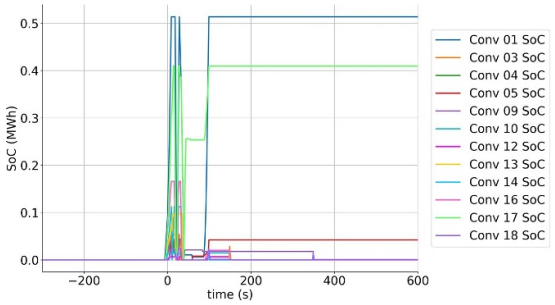

Figure 2. SoC of converter energy storage in reference case.

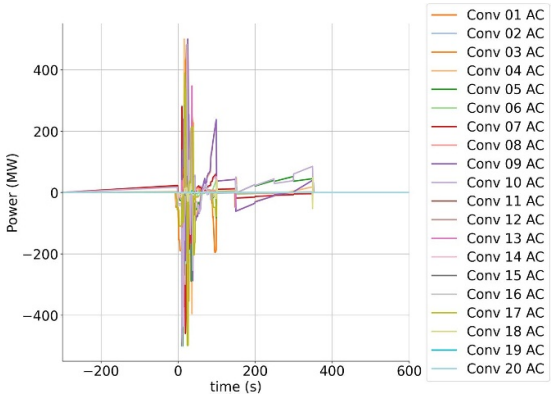

Figure 3. Electrical power exchange at the front-end (grid-side) of all coil converters in the reference case.

The total active pulsed-power and total grid connection limits are shown in figure 4 along with the more restrictive limits resulting from the additional demand imposed by HCD, and the according total PF/CS demand, mitigated by energy storage distributed across converters.

The rate-of-change of grid connection active power, limited to within ± 50 MW s^{-1} by the application of energy storage distributed across multiple converters is shown in figure 5.

It has been demonstrated that, by the optimised distribution of approximately 1.52 MWh across a subset of PF/CS coil converters, pulsed active power grid demand may be constrained to $+/-500$ MW, with a maximum rate-of-change of grid power of 50 MW s^{-1}. Whilst the required ratings of individual coil converters is challenging, with a maximum instantaneous coil power exchange for any single coil of approximately 500 MW, in the reference case, the distribution of 1.52 MWh

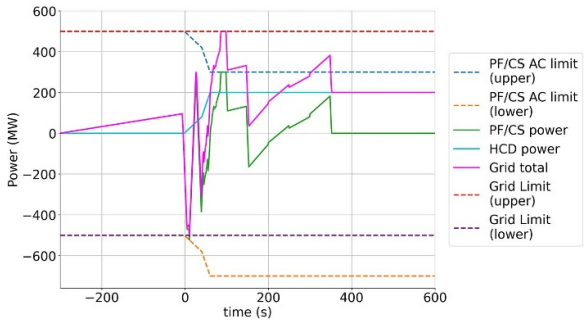

Figure 4. Total PF/CS power profile mitigated by distributed storage and HCD power profile from reference case, with resulting grid connection power profile.

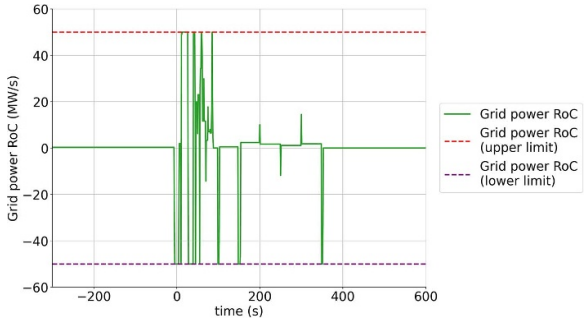

Figure 5. Grid connection rate-of-change of power, mitigated to within limits by distributed storage.

of storage across multiple converters is considered a realistic solution to the mitigation of grid connection constraints.

For the purpose of this analysis, we have assumed ideal performance of the storage elements. Whilst round-trip efficiency of EDLCs is typically high, in the order of 90%–95%, these losses would need to be budgeted for in subsequent design stages, and storage capacity oversized accordingly.

2.4. Electrical power distribution system preliminary architecture and design

The applicability of commercially available power distribution equipment to the design of a future fusion power plant is assessed by creating a preliminary power distribution system architecture design, using the previously electrical loads characterisation and other industry standard planing and equipment sizing criteria [4, 12, 13].

A model of the ST-E1 electrical distribution network (to supply both the steady state loads and the pulse power ones) has been developed in PSCAD. At present, it allows running power flow simulations to support sizing of main electrical components and check voltage variation limits on distribution nodes. In the future it will allow the integration of already developed custom models for coil power supplies and tokamak magnetically coupled coil magnet system with externally supplied current profiles, thus bridging the domains of power distribution and tokamak magnet systems. The model will allow performing further electrical specific studies, including checking electrical generator connection compliance with transmission grid requirements.

Grid connection of the ST-E1 pilot plant is assumed to be at extra-high-voltage transmission level of 400 kV, with the precise requirements dependent on the local network topology, fault-level studies and compliance with transmission system operator Grid Code requirements [25]. A high short-circuit ratio is required at the grid connection point, to tolerate the overall power profile of the plant, which includes a rapid ramp of demand during pulse startup, subsequently transitioning to net power export during the pulse flat-top. A high-voltage substation, part of the main transmission grid, is the connection point for both the plant's generator and the plant's internal distribution system.

The proposed high-level architecture of the plant's electrical distribution network is shown in figures 11 and 12. The configuration with the previous chosen number of transformers and this voltage level is economic, provides a lower site footprint than other options (lower voltage levels but with a higher number of smaller transformers) and already assumes a minimum security of supply.

The final HV distribution voltage is chosen based on the final loads requirements, with transformers rated accordingly, to satisfy installed load capacity, voltage limits in all steady-state and transient operation and security of supply. For the Steady State network, the 33 kV voltage is used to provide an intermediate open ring bus with lower short circuit capacity, providing space for further refining downstream distribution, while still allowing commercially available sized circuit breakers to be used. The same rationale is applied for the 132 kV intermediate Pulsed Power network. For the Steady State network, the other HV levels are chosen based on the size of the largest loads, voltage drop and commercial availability of switching equipment. For the Pulsed Power network, the final voltages reflect the size of the largest magnet and HV gyrotron's power supplies, with further refining taking place once power supply design becomes more advanced.

The electrical loads that support the continuous operation of the plant are fed from the HV transmission substation, using oil-insulated step-down transformers, stepping down the voltage to an intermediate level of 33 kV, with the help of three 200 MVA transformers (for the IHL thermal management architecture) and five transformers (for the CHL thermal management architecture). This intermediate voltage level allows transformer reserve capacity for two intermediate buses at 33 kV. A second set of transformers step down the voltage to a lower level of 13.8 kV and 6.9 kV for final distribution to individual loads, local power centres or low voltage substations. The choice of intermediate voltage levels was supported by low flow studies and industry standard technical and economical criteria limits [4, 12].

Operating two lower HV levels is easily achieved by replacing the final HV transformers with similar three-winding ones, once the exact load distribution between the two levels is known. 13.8 kV was chosen as the second HV distribution level, to allow greater flexibility when future loads will be

refined. Also, these buses will supply other medium voltage to low voltage transformers and switchgear at 0.4 kV or 0.69 kV, which are installed in multiple locations around the site, to supply the majority of smaller electrical plant items. In the initial planing of the distribution system, all loads are lumped to account for the values assumed for the load survey.

The high level topology of the SSEN mirrors the established standards for a classical power generation plant, and assumes the existence of at least one 'Unit' bus, with one fed from the generator output and one from the off-site grid transmission substation.

In common with the segregated network structure assumed earlier, two separate feeders from the HV transmission substation, are used to supply two independent transformers 400 kV / 132 kV, 350 MVA each, for loads associated with the PPEN. The topology of this distribution system assumes there is an intermediate HV substation, 132 kV, with a double busbar system. The two busbars group both magnet and ECRH power supplies, with a various number of power supplies distributed across the two, such as the total demand, during the breakdown and flattop phase of the pulse, is kept as uniform and less variable as possible.

The two main groups of power supplies (magnet and ECRH cathode) have different requirements in terms of supply parameters, owing to their different topology, rated powers and voltages. To get similar loading on each of the two transformers, each 132 kV busbars supply a mix of magnet and ECRH power supplies. The magnet power supplies are distributed across four 33 kV buses, fed by 150 MVA transformers, with the optimum distribution of the 20 converters still under analysis. Because the peak power demand of most converters is large compared to the mean demand during a pulse, and this demand has a very transient nature, there is place for further optimisation of the transformer's size while taking into account a different duty-rating that closer matches the pulsed nature of the loads. The ECRH HV power supplies are uniformly distributed across four 11 kV buses with, fed by 50 MVA transformers. The smaller capacity of these power supplies makes the supply distribution at lower levels economical.

Based on the preliminary design of the electrical power distribution system of the ST-E1 plant and assuming novel designs for power electronic converters of the the magnet power supplies and ECRH HV cathode power supplies, commercial power distribution equipment and industry standardised technologies can be used for a future fusion-enabled power plant, with enough room for further optimisation of equipment ratings, which can further slightly lower the recirculating power associated with the Electrical Systems.

3. Power out

To evaluate the power generated by ST-E1, it is necessary to characterise the thermal power outputs and the overall thermal system integration. The RDP specifies both surface and volumetric heat fluxes that the in-vessel components of the tokamak must accommodate. In parallel, the thermal-hydraulic integration of the coolant loops across the various subsystems, together with the design of the power generation system, is configured so as to minimise pumping power requirements and maximise the utilisation of the available heat in ST-E1. These thermal systems are subsequently coupled to the electricity generation systems that determine the plant's gross electrical output, thereby defining a key contribution to the net plant power balance. At this stage, solely the steady-state loading for these components has been defined.

3.1. Heat sources in ST-E1

The fusion island of ST-E1 employs two primary coolants—helium and liquid lithium—to remove heat from the breeder blanket, divertor and CCS regions. These fluids constitute the primary heat extraction loops that transfer thermal power to secondary systems. The choice of coolants was due to several factors, but the compatibility of the materials, especially at high temperatures, is a key driver because environmental degradation is a potentially limiting factor that can limit the upper operating temperature of a fusion component [26]. In the absence of environmental effects, nuclear structural materials tend to have an operational temperature window bound at the low end by hardening and embrittlement and either creep deformation or helium embrittlement at the high end [26]. As a result, coolant inlet and outlet temperatures for components in ST-E1 tend to be driven by constraints imposed by materials. In ST-E1, fusion energy is captured in three main regions: the breeder blanket, divertor and CCS. This section summarises analyses of their respective contributions for use in the plant's thermal balance.

3.1.1. Breeder blanket. In ST-E1, the low aspect ratio restricts breeding to the outboard region, so lithium compounds with a high tritium breeding ratio (TBR) are preferred. To obtain sufficient TBR without using a neutron multiplier such as beryllium and lithium enrichment, liquid lithium, with natural isotopic abundance, was selected for the breeder blanket. The structural material selected for the breeder blanket, due to its compatibility with liquid lithium and high neutron transparency, is V–4Cr–4Ti (V44), which has a safe operating window of ∼400 to 700° [26]. Initially, liquid lithium was considered as the primary coolant for the system. However, its large mass flow requirement and high electrical conductivity induce strong Magneto-Hydrodynamic (MHD) effects, which can create operational difficulties. Therefore, helium was selected as a secondary coolant for cooling the breeder blanket's first wall and to extract a portion of the volumetric nuclear heating. The helium inlet temperature is maintained at 400° to prevent significant irradiation hardening and embrittlement of the V44 structure. Potassium doped tungsten (K-doped W), which has an operational temperature range of ∼350 to 850–1100°, is used as the plasma facing armour [27, 28]. During pulse/flattop operation, the blanket will experience 200 MW of surface heating from a plasma

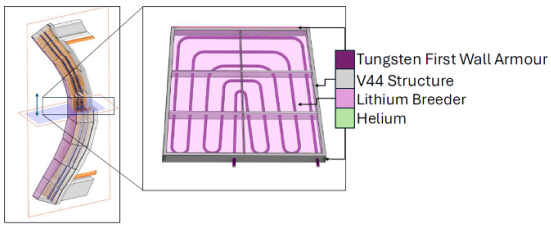

Figure 6. Breeder blanket slice cross-section.

Table 3. Breeder blanket temperatures.

	K-doped W	V44	Lithium
Purpose	Armour	Structure	Breeder
Average temperature (°C)	573	487	588
Minimum temperature (°C)	533	401	424
Maximum temperature (°C)	611	671	765

heat flux of 0.4 MW m^{-2} and 1050 MW of heating from neutron energy deposition as calculated using OpenMC—a Monte Carlo transport code [29]. Additional details on the breeder blanket design is covered in an accompanying paper [30].

To cool the first wall, square helium channels are integrated into the V44 structure, directing the flow from the rear of the blanket across the front wall at a velocity of 60 m s^{-1} and a pressure of 80 bar. To enhance the heat transfer, it is assumed that turbulent ribs can be incorporated adjacent to the front wall, potentially doubling the local heat transfer coefficient [31].

Each 105 mm-thick blanket slice incorporates four square ducts (a cross-section of a breeder blanket slice is shown in figure 6). The outlets from two of the ducts are routed into the inlets of the remaining two, allowing the helium to pass along the first wall twice. The outlets of this second pair are then combined and directed into a downstream pipe, where heat is removed from the lithium volume. This arrangement is intended to maximise cooling effectiveness, enhance the helium temperature pick-up, and lower the total helium mass flowrate requirement.

Thermal analyses were conducted to optimise the pipe network and maximise the helium temperature rise for power generation, with the outcomes summarised in table 3. The data confirm that the proposed cooling configuration keeps all material temperatures within allowable operating limits while producing a 205° helium temperature increase, suitable for power generation.

Although the dual-cooled helium–liquid lithium concept is the baseline breeder blanket design for ST-E1, a self-cooled liquid lithium option could largely reduce parasitic loads by eliminating the need for helium coolant and its associated pumping power requirements. An initial assessment of a *slotted* channel arrangement that lowers the required lithium mass flowrate, following the approach in [32], has been conducted. Using the Hunt solution for magnetohydrodynamic duct flow to estimate first-wall cooling [33], the predicted pressure drop across the slotted channel is approximately 1000 Pa at a lithium velocity of 1.5 m s^{-1}. The corresponding pumping power is significantly lower than that for helium cooling under comparable conditions. Realising this concept will require several years of development, including high-fidelity 3D simulations and experimental validation.

3.1.2. Divertor. The tokamak's divertor is responsible for intercepting the majority of the charged particles and heat flux that leaves the confined area of the plasma. The heating power, $P\alpha$, that leaves the core this way (i.e. the non-neutronic power) is equal to 20% of the fusion power, plus the auxiliary power input from HCD or inductive heating. Because ions travel along field lines more readily than across them, the plasma exiting the core transports this power to the divertor in a very thin layer. If this was not mitigated in any way, it typically leads to heat fluxes on the order of 100–1000 MW m^{-2} in a small stripe on the divertor. Given that the surface cooling capability of the plasma facing component (PFC) is typically limited to the order of 10 MW m^{-2}, a significant amount of the power must be shed from the leg via EM radiation. Some of this will fall on the blanket and centre column, and some will fall on the divertor itself.

For the purposes of the analysis in this paper, the divertor power input to the power generation system will be allowed to vary according to the radiation needed for each divertor type. There is still uncertainty in which PFC technology will be used for the divertor, while the breeding blanket and centre column designs are better understood. Therefore, the inputs for the latter were frozen before that of the divertor to allow further analysis. As a result, changing fractions of power radiated to the blanket first wall are not captured here, and this makes the analysis slightly conservative with respect to overall thermal power for some divertor configurations. In the results shown, this represents an omission of ∼5% of thermal power, which should be acceptable given the maturity level of the pre-concept design.

Two PFC technologies have been selected for investigation in the pre-concept stage: the HEMJ [34], and a proprietary heat pipe-based concept referred to here as HP-PFU. To allow power cycle integration, data from literature [35] was used to characterise the required mass flow and pressure drop for using HEMJ at various heat fluxes up to 10 MW m^{-2}. HP-PFU is at an early stage of development, but some assumptions were made to allow derivation of the same properties for a representative design. Based on [34], the HEMJ design is assumed to use a tungsten alloy (La_2O_3-doped W) for the coolant pressure boundary. This material imposes a minimum coolant inlet temperature of 600° to ensure that the walls retain their ductility. The HP-PFU is assumed to use V44 for its pressure boundary, giving a minimum coolant temperature of 400°. Both technologies are assumed to have the same maximum outlet temperature of 700°, based on the assumed use of V44 as the manifold material.

Multiple possible layouts of divertors made using these two technologies were compared to assess the overall pressure

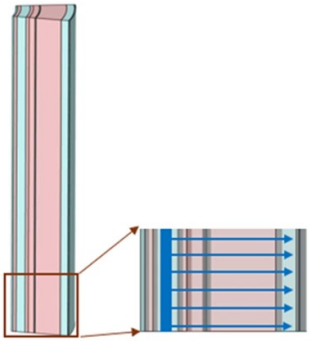

Figure 7. Schematic diagram of the cooling scheme adopted for the CCS.

drop, pickup temperature, and mass flowrate of each (further details are covered in an accompanying paper [36]). A full optimisation of the divertor layout was not possible in the scope of the pre-concept design and is left to future work. Overall, however, the HEMJ has less flexibility for optimisation due to its high required inlet temperature (hence low allowable pickup temperature) and its high pressure drop for a given heat flux (due to its use of jet impingement as a means of achieving high heat transfer coefficient). Meanwhile, the HP-PFU has a lower inlet temperature, allowing for a higher overall pickup temperature. Furthermore, its operating principle is to use a heat pipe to spread the high plasma heat flux peak over a larger coolant surface area, resulting in a lower pressure drop for a given heat flux.

3.1.3. Centre Column Shield (CCS). The CCS attenuates the flux of ionising radiation on the reactor components, such as the HTS magnets and the vacuum vessel. Approximately 12% of the reactor's total thermal power is deposited on the CCS by neutron flux and plasma heating. Extracting this energy as high-grade heat can improve the overall power balance of the plant, provided it is recovered at temperatures compatible with the power generation system.

Figure 7 illustrates the thermal management configuration adopted for the CCS. The design employs a radial-plane cooling scheme, in which a central manifold distributes coolant to the shielding along the radial plane.

The material selection for the CCS is based on the required shielding performance while ensuring that the shielding materials remain encapsulated within the structure for the entire lifetime of the CCS. The chosen shielding material is tungsten carbide (WC) [37, 38]. Similar to the breeder blanket, the structural material is V44 and the plasma facing material is K-doped tungsten. During pulse/flattop operation, the CCS will experience a total power load of 200 MW, of which 150 MW arises from neutron energy deposition and 50 MW from plasma heat flux. This figure includes heat deposited onto the outboard horizontal shields [38].

The concept developed to meet the shielding requirements and manage the plasma heat flux consists of a structure that houses high-performance shielding blocks. Coolant channels are integrated into the structure, allowing helium to circulate and remove heat from both the shielding blocks and the first wall. The helium flows through these channels at a velocity of 50 m s^{-1}, 400 °C inlet temperature and a pressure of 80 bar. Similar to the breeder blanket, to enhance heat transfer, it is assumed that turbulent ribs can be incorporated adjacent to the front wall.

Table 4. Centre Column Shield temperatures.

	K-doped W	V44	Tungsten carbide
Purpose	Armour	Structure	Shield brick
Average temperature (°)	644	540	676
Minimum temperature (°)	525	400	401
Maximum temperature (°)	750	722	1058

Thermal analyses were conducted to optimise cooling channel dimensions and maximise the coolant outlet temperature. Table 4 shows the resulting CCS average and maximum temperatures. These results demonstrate that the proposed cooling solution maintains all material temperatures within acceptable operational limits, while achieving a 114 °C temperature rise in the helium.

3.2. Heat extraction systems

A summary of the coolant requirements for the breeder blanket, divertor and CCS is shown in table 5. The elevated coolant temperature and pressure conditions required by the reactor components necessitate the design of coolant loops capable of efficiently removing high heat fluxes while maintaining component temperatures within the allowable limits imposed by the properties of the structural materials.

A major design challenge for the helium coolant loop is the need for very high mass flowrates to achieve the necessary heat removal under the specified operating conditions. Similar to helium, lithium is circulated at elevated conditions. During operation, the loop must also accommodate interactions with tritium extraction and purification systems, which require controlled flow routing and thermal management to ensure effective tritium recovery without compromising heat removal performance. Temperature and pressure regulation is achieved through dedicated liquid metal pumping systems and heat exchangers.

3.2.1. Integration with the power cycle and the need for a thermal buffer. The primary coolant loops can be integrated with the power generation system either through direct coupling or via an intermediate thermal buffer medium. Each configuration presents distinct advantages and trade-offs. In a directly coupled arrangement, the hot coolant is routed from the reactor components to heat exchangers, where it transfers thermal energy directly to the power generation cycle working fluid. After heat exchange, the coolant passes through heat recovery, compression, and purification systems before being recirculated to the reactor. In contrast, in the the indirectly coupled configuration, the hot coolant first transfers heat to the

Table 5. Summary of thermal power extraction from ST-E1.

	Breeder blanket	Centre column shield	Divertor	
			HP-PFU	HEMJ
Extracted thermal power	1252 MW	200 MW	242 MW	158 MW
Coolant(s)	Lithium & Helium	Helium	Helium	Helium
Mass flowrates	292 kg s^{-1} (lithium) & 962 kg s^{-1} (helium)	338 kg s^{-1}	212 kg s^{-1}	565 kg s^{-1}
Inlet temperature	400 °C	400 °C	400 °C	600 °C
ΔT	188 °C (lithium) 205°C (helium)	114 °C	220 °C	54°C
Pressure drop	10 bar (lithium) 4 bar (helium)	1.37 bar	10.5 bar	16.5 bar

buffer medium, which is then used to heat the working fluid of the power cycle.

The direct coupling approach offers several advantages. High-grade heat from the fusion island can be directly transferred to the power cycle working fluid, enabling higher operating temperatures and, consequently, improved thermal-to-electric conversion efficiency. Furthermore, the elimination of intermediate loops minimises parasitic losses associated with pumping secondary heat transfer fluids or thermal buffer media. However, the direct coupling approach introduces several challenges. The power generation system becomes tightly coupled to the reactor operating conditions, reducing operational flexibility and complicating grid integration—particularly in the pilot phase where continuous steady-state reactor operation may not be established. Additionally, the potential for tritium contamination in the working fluid poses significant safety and regulatory concerns. Finally, this configuration limits design modularity, making it more difficult to isolate or upgrade the power conversion system without impacting reactor operations.

Introducing a thermal buffer offers key system-level benefits. It decouples the power cycle from reactor dynamics, enabling smoother thermal energy delivery and enhancing grid compatibility. The buffer also minimises contamination risks and reduces thermal transients impacting the power cycle. While incorporating a thermal buffer enhances system reliability, it introduces additional thermal energy losses due to the extra heat transfer steps required. The temperature bound of the power cycle's working fluid is also constrained by the operational limits of the thermal buffer material. As a result, the power cycle may operate at a lower temperature than it would if directly coupled to the reactor, leading to reduced thermal-to-electrical power conversion efficiency. Nonetheless, this trade-off is justified by the improved reliability, maintainability, and operational flexibility of the overall power generation system, especially during the pilot phase of ST-E1.

Molten salts have emerged as a promising choice for thermal energy storage due to their high energy storage capacity, exceptional thermal stability, scalability and cost-effectiveness [39]. Molten salts are widely used in commercial concentrated solar power plants [40] and are a promising candidate for the production of fusion power due to their favourable thermo-physical properties at high temperatures. Commonly used molten salts for heat storage applications are solar and HITEC salts. Solar salt was selected as the thermal buffer medium for ST-E1 with an operational temperature range of 290 °C–565 °C. While various studies report differing upper operational limits for solar salt, a temperature of 565 °C is widely accepted as the practical maximum for current thermal energy storage (TES) systems [41]. Solar salt solidifies at relatively high temperatures of ∼240 °C [42] so 290 °C was selected as a suitable lower operating temperature bound.

3.2.2. Thermal management process architecture. The aforementioned information was consolidated into two alternative process architecture models (IHL and CHL) built with Aspen HYSYS® [43]. These two versions exist to accommodate the two different proposed divertor design options. IHL employs the HP-PFU divertor, whereas CHL employs the HEMJ divertor.

The resulting process architecture models are shown in figures 13 (IHL) and 14 (CHL). The lines represent the material streams: helium (black), lithium (purple) and solar salt (orange). The process consists mainly of the following equipment: heat exchangers, compressors, pumps, storage tanks, and feed mixers/splitters. The primary distinction between the two design versions lies in the configuration of the divertor coolant loops. As the required helium mass flowrate and inlet temperature for the divertor varies with the chosen divertor concept, the IHL architecture employs an IHL dedicated to divertor cooling. In contrast, the CHL architecture utilises a portion of the helium flow from the breeder blanket to cool the divertor, coupling the breeder blanket and the divertor in a single coolant loop. This approach is driven by the high inlet temperature requirement of the HEMJ divertor.

Pressure drops and coolant pumping requirements. Helium's low density, even at elevated pressures, results in large volumetric flowrates, which in turn demand significant pumping power. Helium systems are particularly sensitive to pressure drops due to the high compression power required. In the reactor components, helium experiences pressure drops across the manifolds and cooling channels of the breeder blanket, CCS and divertor. Beyond the reactor components, the helium loop incorporates a large number of heat exchangers required to manage temperature across various stages of the system. Additionally, the plant-wide piping network contributes to cumulative pressure losses.

Table 6. Heat exchanger pressure drops.

	Helium	Lithium	Solar salt
Helium-solar salt HX	2–3.7 bar	—	0.1–1.9 bar
Helium–lithium HX	2.6 bar	0.5 bar	—
Helium recuperators	2.2–5 bar (shell-side) 0.2–0.3 bar (tube-side)	—	—
Helium coolers	1–1.9 bar	—	—

Table 5 summarises the pressure losses for both helium and lithium in the reactor. These values represent the total calculated pressure drops experienced by the coolants as they flow through the reactor's cooling channels.

Heat exchangers represent another significant source of pressure drops within the system. For simplicity in modelling, each heat exchange block has been represented by a single heat exchanger; however, in practice, these blocks would be divided into multiple heat exchangers arranged in series and parallel configurations to accommodate the large helium mass flowrates. Aspen Exchanger Design & Rating™ [44] software was used to estimate the pressure drops across the heat exchangers, with the results summarised in table 6. These values represent the total pressure drop for each heat exchanger block, which includes the combined pressure losses from all individual heat exchangers within that block. These results were incorporated in the process models, as they play a critical role in determining the required pumping power.

To maintain the required pressure level of 80 bar inlet pressure to the reactor and ensure adequate mass flow supply, the helium loop incorporates multi-stage centrifugal or axial compressors, often equipped with inter-cooling to limit temperature rise and improve efficiency. Their electrical power demand represents a significant fraction of the plant's recirculating power, making compressor efficiency a key factor in overall plant performance. The helium compressor modelling relied on several assumptions, including a stage pressure ratio of 1.032, consistent with the helium compressor turbine design in a 300 MW HTGR-GT (High-Temperature Gas-Cooled Reactor—Gas Turbine) plant [45]. The same stage pressure ratio was applied to verify the simulation methodology for a highly loaded helium compressor of a closed Brayton cycle HTGR power plant [46]. A review of axial helium compressors for HTGR reactors reported isentropic efficiency values ranging from 87% to 89% [47]. The authors note that there remains potential for improvement, with state-of-the-art helium compressors expected to achieve even higher efficiency levels.

Based on these assumptions and for the given pressure drops, the total helium compression power requirements were calculated to be 220 MW for the IHL architecture and 357 MW for the CHL architecture, respectively, with compression pressure ratios of 1.1–1.7 at 50 °C.

A sensitivity analysis was conducted to assess how the variation of the inlet temperature of helium to the compressor affects the required compression power, as illustrated in figure 8. The results show a linear increase in compression power with rising inlet temperature, assuming constant isentropic efficiency. This trend is primarily driven by fundamental gas dynamics: as helium temperature increases, its density decreases, necessitating a higher volumetric flowrate to maintain the same mass flow. This increase in flow volume directly translates to greater compression work.

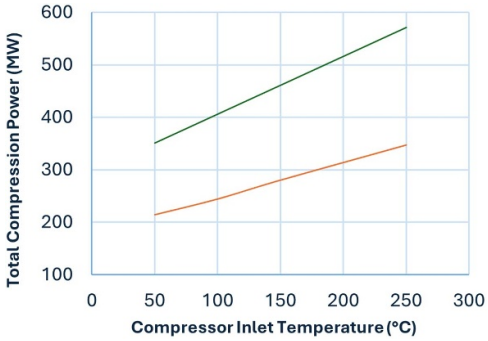

Figure 8. Effect of varying compressor inlet temperature on compression power. IHL (orange) and CHL (green).

These findings suggest that selecting a lower compressor inlet temperature is advantageous. The reduction in compression power requirements significantly reduces the auxiliary power demand of ST-E1, which is a critical parameter in net power calculations and a key determinant of the overall viability of the plant. In addition, operating at reduced temperatures simplifies the design requirements of the compressor, as the system can be optimised for less demanding thermal conditions and reduced inter-cooling needs.

As expected, helium compression was identified as one of the dominant contributors to the system's auxiliary loads, accounting for over 95% of the total pumping power requirements. This contribution was even higher in the CHL architecture, primarily due to the increased pressure drop across the HEMJ divertor. This makes helium compression a critical aspect of the overall net power balance, as its performance directly influences the system's efficiency and viability.

EM pumps are the preferred technology for circulating liquid lithium in fusion breeder blanket systems due to their ability to operate at high temperatures without moving parts, thereby minimising wear and sealing challenges. Among the available designs, annular linear induction pumps (ALIPs) and conduction pumps have demonstrated suitability for high-flow, high-temperature applications. However, they have lower efficiency than mechanical pumps, typically 5%–45%, due to resistive losses and geometric effects, though design optimisations can improve performance [48]. The required lithium

Table 7. ST-E1's thermal fluids' properties.

	Helium (400 °C–700 °C)	Lithium (400 °C–600 °C)	Solar salt (290 °C–565 °C)
Density (kg m^{-3})	5.67–3.93 [49]	502–522 [50]	1907–1730 [51]
Specific heat capacity (Jg·C^{-1})	5.19 [49]	4.17 [52]	1.52 [51]
Viscosity (Pa·s)	35.0–45.4 × 10^{-6} [49]	3.42–4.54 × 10^{-4} [50]	1.14–3.56 × 10^{-3} [51]
Thermal conductivity (Wm·C^{-1})	0.28–0.36 [49]	51.4–57.0 [50]	0.53 [51]

pumping power obtained from the simulation for ST-E1 is 4 MW for a pressure ratio of 10.3 at 20% efficiency.

Heat exchanger network. To optimise heat recovery within the system, pinch analysis was utilised with two primary objectives: to eliminate the need for auxiliary heating of coolant during steady-state operation, and to minimise heat rejection to external heat sink. This approach enabled the identification of thermodynamically favourable heat exchange opportunities, ensuring that available thermal energy is effectively reused within the system, reducing overall energy losses.

For the process modelling and pinch analysis, several assumptions were made. All heat exchangers in the system were assumed to be of the shell-and-tube type, which facilitated the estimation of pressure drops across the heat exchanger network-an important factor in determining pumping requirements, particularly for helium. Also, for the pinch analysis, a minimum temperature difference of 10 °C was assumed. The specific heats were assumed to be constant, and heat transfer to the surroundings was assumed to be negligible.

The properties used for helium, liquid lithium and solar salt in the process modelling are shown in table 7.

Hot helium from the fusion island is directly used to heat the 'cold' solar salt, following a configuration defined by the heat exchanger network design. All heated solar salt streams are directed into the hot tank at a temperature of 565 °C. For modelling simplification, the system has been represented using a single hot and cold tank; however, in practice, multiple tanks would be required to accommodate the full inventory of solar salt.

A lithium-helium heat exchanger has been incorporated to cool the lithium exiting the breeder blanket from 588 °C to 400 °C, enabling its reuse within the blanket or further processing through tritium extraction and purification systems. In addition to cooling the lithium, the heat exchanger preheats the helium entering the breeder blanket to 400 °C, improving overall thermal efficiency of the process.

The return helium streams are directed to the compression loops, which consist of recuperators, coolers, and compressors. These loops are configured to manage helium temperatures before and after compression, ensuring that the helium is supplied to the compressor and returns to the reactor components at the required temperature conditions. The combination of a high reactor inlet coolant temperature and a comparatively lower compressor inlet temperature necessitates an effective heat recovery strategy.

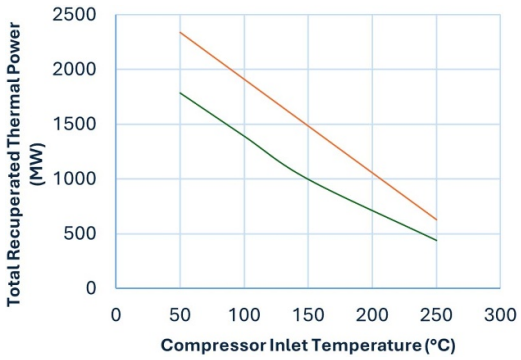

Figure 9. Effect of varying compressor inlet temperature on recuperation duty. IHL (orange) and CHL (green).

The extent of heat recovery required in the system is closely linked to the operating temperature of the helium compressors. Lower compressor inlet temperatures necessitate larger and more complex heat recovery systems, increasing the number and size of heat exchangers and associated infrastructure. Conversely, operating compressors at higher inlet temperatures reduces the demand on the heat recovery system but significantly increases the compressor power requirements and may present challenges with compressor design. Therefore, a careful balance must be struck between the size and complexity of the heat recovery system and the electrical power consumed by the compressors, with implications for both system design and net plant performance.

Although 50 °C was selected as the compressor operating temperature due to the relatively low compression power requirement, a sensitivity analysis was performed to examine how compressor inlet temperature affects the total recuperated thermal power, as shown in figure 9. For example, when the compressor inlet temperature is set to 50 °C, the total required recuperation duty for the IHL architecture is approximately 2300 MWth (Megawatt thermal). In contrast, increasing the compression temperature to 250 °C reduces the recuperation duty to ∼630 MWth. This substantial difference has significant implications for the overall system design. Therefore, recuperation requirements must be carefully considered when selecting the compressor design temperature target.

3.3. Electrical power generation

The chosen power cycle for ST-E1 is an advanced supercritical Rankine cycle. Traditionally employing steam as the working

fluid, the Rankine cycle is a well-established and commercially mature technology widely used in conventional thermal power plants. Advanced Rankine cycles represent a significant evolution over the conventional Rankine cycle, offering enhanced thermal efficiency and improved adaptability to high-temperature heat sources such as those from fusion reactors. These advanced configurations usually incorporate features such as supercritical/ultra-supercritical steam conditions, reheat stages, regenerative feedwater heating, and organic working fluids. By operating at higher pressures and temperatures, advanced supercritical/ultra-supercritical Rankine cycles can achieve efficiencies exceeding 45%, compared to 30%–35% for traditional subcritical systems.

The steam cycle was modelled in Aspen HYSYS as shown in figure 15. Heat is transferred to the power generation cycle via water/steam-solar salt heat exchangers. These exchangers comprise of steam generators, superheaters, and reheaters. Hot solar salt first enters the steam superheater and reheater stages, after which it is directed to the steam generators. The quantity of solar salt circulating in the thermal buffer loop was selected to enable steam generation at 550 °C; a temperature considered achievable within the operational limits of solar salt [53].

The selected advanced steam cycle incorporates three steam turbines (high-, intermediate- and low- pressure). It also features regenerative feedwater heating, where steam is extracted from turbine stages to heat the feedwater via a combination of open and closed feedwater heaters. However, because direct turbine bleeding was not available within the modelling framework, an approximation was implemented by dividing the high-pressure turbine into two modules, with the split occurring at the conditions corresponding to the required bleed point. The same approach was applied to the intermediate- and low-pressure turbines to replicate the thermodynamic behaviour of steam extraction and ensure accurate cycle performance representation.

Although steam cycles typically employ a larger number of feedwater heaters for efficiency, this design simplifies the arrangement by incorporating four closed feedwater heaters and one open feedwater heater. The following parameters were used in the steam cycle:

- Main steam temperature and pressure: 550 °C and 230 bar
- Steam reheat temperature: 550 °C
- Condenser pressure: 0.045 bar

The resulting efficiency from the steam cycle was 47.2%.

4. Producing net power

To assess the viability of ST-E1 in achieving a positive electrical net power output, a comprehensive power-balance analysis must be performed. This analysis quantifies the difference between the gross electrical power generated by the power conversion system and the total electrical power consumed by the plant's subsystems and auxiliary components. Ensuring a positive margin in this balance is critical for demonstrating the plant's capability to deliver net electricity to the grid.

Four distinct scenarios are analysed to evaluate the capability of ST-E1 to meet the overall plant performance requirements. These scenarios span the two divertor configurations described previously and two flattop ECRH powers: 100 MW, derived from preliminary current ramp-up simulations, and 75 MW, which corresponds to the RDP. Across all scenarios, the breeder blanket concept and the centre column shielding configuration are held fixed.

The four cases are:

- Case 1: HP-PFU divertor, 100 MW ECRH
- Case 2: HP-PFU divertor, 75 MW ECRH
- Case 3: HEMJ divertor, 100 MW ECRH
- Case 4: HEMJ divertor, 75 MW ECRH

The total thermal power extracted from the reactor during the flattop phase, P_{th}, is defined as the sum of the individual thermal power contributions extracted from the breeder blanket, the divertor, and the CCS. The underlying calculation methodology for these contributions has been discussed in detail in the preceding sections and is summarised in table 5.

For ST-E1, steady-state operation is taken as the reference mode. The steady-state net electrical output, $P_{\mathrm{net,SS}}$, is given by the difference between the gross electrical power generated by the power generation system in steady-state conditions, $P_{\mathrm{out,SS}}$, and the internal power recirculated to maintain the plasma and auxiliary systems, $P_{\mathrm{rec,FT}}$. The steady-state thermal power input to the power generation system, $P_{\mathrm{th,SS}}$, is the total thermal power extracted during flattop, P_{th}, minus thermal losses in the heat transfer process. The total thermal power comprises the energy deposited by fusion products (neutrons and alpha particles), together with thermal contributions from auxiliary plasma-heating systems. Under these assumptions, the resulting net power outputs are listed in table 8.

Case 2 delivers the highest steady-state performance at 335 MWe, comfortably within the pilot-phase target range. Case 1 follows with 278 MWe, which is close to the threshold but may require incremental improvements in efficiency or reduced auxiliary loads to ensure viability. In contrast, cases 3 and 4 deliver lower outputs, emphasising the need for targeted design refinements and optimisation to enable effective integration of the HEMJ divertor concept into the plant architecture.

A comprehensive Sankey diagram illustrating the complete energy flow throughout the ST-E1 plant is presented in figure 16.

Although steady-state operation is the reference mode, pulsed operation may be required in this largely unexplored regime. In such a case, the 300–500 MWe target would represent the average net electrical output over the reactor duty cycle, defined as the full sequence of operation divided into four distinct phases:

1. **Ramp-up**, during which plasma parameters are increased to achieve nominal operating conditions;
2. **Flattop**, or pulse, where sustained plasma burn occurs for energy production;
3. **Ramp-down**, involving controlled reduction of plasma current and auxiliary heating;

Table 8. ST-E1 plant power balance summary.

	Term	Symbol	Case 1	Case 2	Case 3	Case 4
Power in	Flattop recirculating power	$P_{\mathrm{rec,FT}}$	483 MWe	426 MWe	625 MWe	568 MWe
	Flattop intermediate recirculating power	$P_{\mathrm{rec,FTi}}$	550 MWe	495 MWe	691 MWe	636 MWe
	Dwell recirculating power	$P_{\mathrm{rec,DW}}$	247 MWe		360 MWe	
Power out	Flattop thermal power produced	P_{th}	1673 MWth		1611 MWth	
Net power (steady-state)	Steady-state thermal power input to the power generation system	$P_{\mathrm{th,SS}}$	1612 MWth		1536 MWth	
	Power cycle efficiency	η_c	47.2%			
	Steady-state gross electrical power output	$P_{\mathrm{out,SS}}$	761 MWe		725 MWe	
	Steady-state net electrical power output	$P_{\mathrm{net,SS}}$	278 MWe	335 MWe	100 MWe	157 MWe

4. **Dwell**, the inter-pulse interval required for thermal recovery and system preparation prior to the next pulse.

Electric system modelling revealed an intermediate stage during the flattop period, after ramp-up, in which the magnets draw extra power after burn has been achieved. This effect is accounted for in the net power calculations and is referred to as the flattop intermediate phase.

Since the flattop phase is the sole period during which the reactor produces positive net power, its duration constitutes a critical determinant of ST-E1's overall net electrical output. Extending the flattop interval directly increases the energy yield per pulse, thereby enhancing the average power delivered over the duty cycle. Consequently, optimisation of the flattop length is a key design parameter to achieve the targeted plant performance.

The thermal buffer is regulated so that the thermal power supplied to the power conversion system remains effectively constant throughout the reactor duty cycle. Consequently, the electrical power output from the power generation system is maintained at a steady and uninterrupted level throughout this period.

The electrical power consumption changes across duty cycle phases. It is taken as constant during the flattop and dwell phases (see table 8), and varies dynamically during the ramp-up and ramp-down phases. It was assumed that electrical power consumption during ramp-down equals that during ramp-up.

Phase energy accounting over one duty cycle is given by

$$E_{XX} = (P_{\mathrm{out}} - P_{\mathrm{rec},XX})\, t_{XX}, \tag{3}$$

where $XX \in \{\mathrm{FT}, \mathrm{RU}, \mathrm{RD}, \mathrm{DW}\}$ denotes flattop, ramp-up, ramp-down, and dwell, respectively,

P_{out} is the constant electrical power output,

$P_{\mathrm{rec},XX}$ is the recirculating (electrical) power for that phase, and

t_{XX} is the phase duration.

The total duty cycle duration is

$$t_{\mathrm{total}} = t_{\mathrm{FT}} + t_{\mathrm{RU}} + t_{\mathrm{RD}} + t_{\mathrm{DW}}. \tag{4}$$

The average net electric power over the duty cycle is then

$$P_{\mathrm{net,avg}} = \frac{E_{\mathrm{FT}} + E_{\mathrm{RU}} + E_{\mathrm{RD}} + E_{\mathrm{DW}}}{t_{\mathrm{total}}}. \tag{5}$$

A dwell-time assumption of 300 s was used in this study, reflecting preliminary subsystem recovery assessments. Figure 10(*a*) illustrates the dependence of the average net electric power output on the flattop duration for the four operational scenarios (cases 1–4). The flattop length represents the sustained high-power phase of the plasma discharge, during which fusion power is generated. The curves exhibit a characteristic asymptotic growth behaviour, reflecting the diminishing returns in average power as the flat-top duration increases.

All cases show a rapid increase in average net electric power for short flattop durations (0–5000 s), followed by a gradual saturation beyond approximately 10 000 s. This trend arises because the ramp-up and ramp-down phases contribute fixed energy penalties, which become negligible as the flattop length dominates the cycle time.

The shaded region (300–500 MWe) represents the net power target for the pilot phase of ST-E1. Case 2 achieves the highest asymptotic power (∼300 MWe), approaching the lower bound of the target range. This underscores the need for extended flat-top durations (>15 000 s) to satisfy pilot-phase objectives under the assumed operating conditions.

Meanwhile, case 1 stabilises near 250 MWe, slightly below the target threshold, suggesting marginal feasibility for commercial deployment without further optimisation. Cases 3 and 4 deliver significantly lower outputs (<150 MWe and <100 MWe respectively), indicating that these configurations are unsuitable for grid-scale electricity generation under the assumed operating conditions. This shortfall is primarily driven by the substantial helium compression power requirements associated with the HEMJ divertor concept.

This analysis highlights the fine margins that can arise when balancing plant loads. It indicates that performance can be improved by: (i) pushing towards higher-Q regimes (reduced auxiliary heating during flattop), (ii) minimising pressure drops across the system (reducing compression duty),

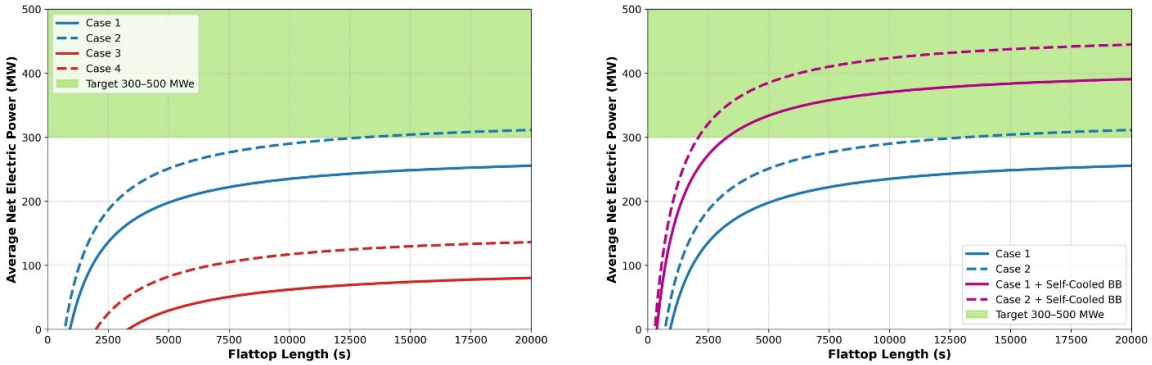

(a) Cases 1-4 (b) Cases 1 & 2 (with self-cooled BB concept)

Figure 10. Average net electrical power with varying flattop lengths.

and (iii) exploring alternative thermal–storage solutions that can improve the efficiency of power generation by increasing the upper temperature of the power cycle fluid. In future stabilised operations, more direct coupling of heat sources to the power conversion system may offer additional efficiency gains.

In the case of pulsed operation, the influence of employing short flattop durations on the structural and mechanical robustness of the reactor and its auxiliary systems must be carefully considered, particularly in light of the sustained thermal and mechanical cycling to which they are subjected. A more comprehensive, dedicated analysis will be required to quantitatively establish the resulting operational constraints, identify potential failure modes, and define acceptable design and operating limits associated with these conditions.

Introducing a self-cooled breeder blanket significantly enhances ST-E1's net electric power performance (see figure 10(*b*)). This modification was applied only to cases 1 and 2, as their divertor and breeder blanket have independent coolant loops. For cases 3 and 4, where both components share a loop, further analysis is required before implementation.

Compared to the baseline, adding a self-cooled breeder blanket provides substantial gains. Both modified cases achieve the 300 MWe target at much shorter flattop durations, whereas their baseline counterparts either fail to reach this threshold or require very long pulses. Overall, the improvement is most pronounced for case 1, which moves from below-target performance to comfortably within the desired range. Case 2 also benefits significantly, achieving higher output at shorter flattop lengths.

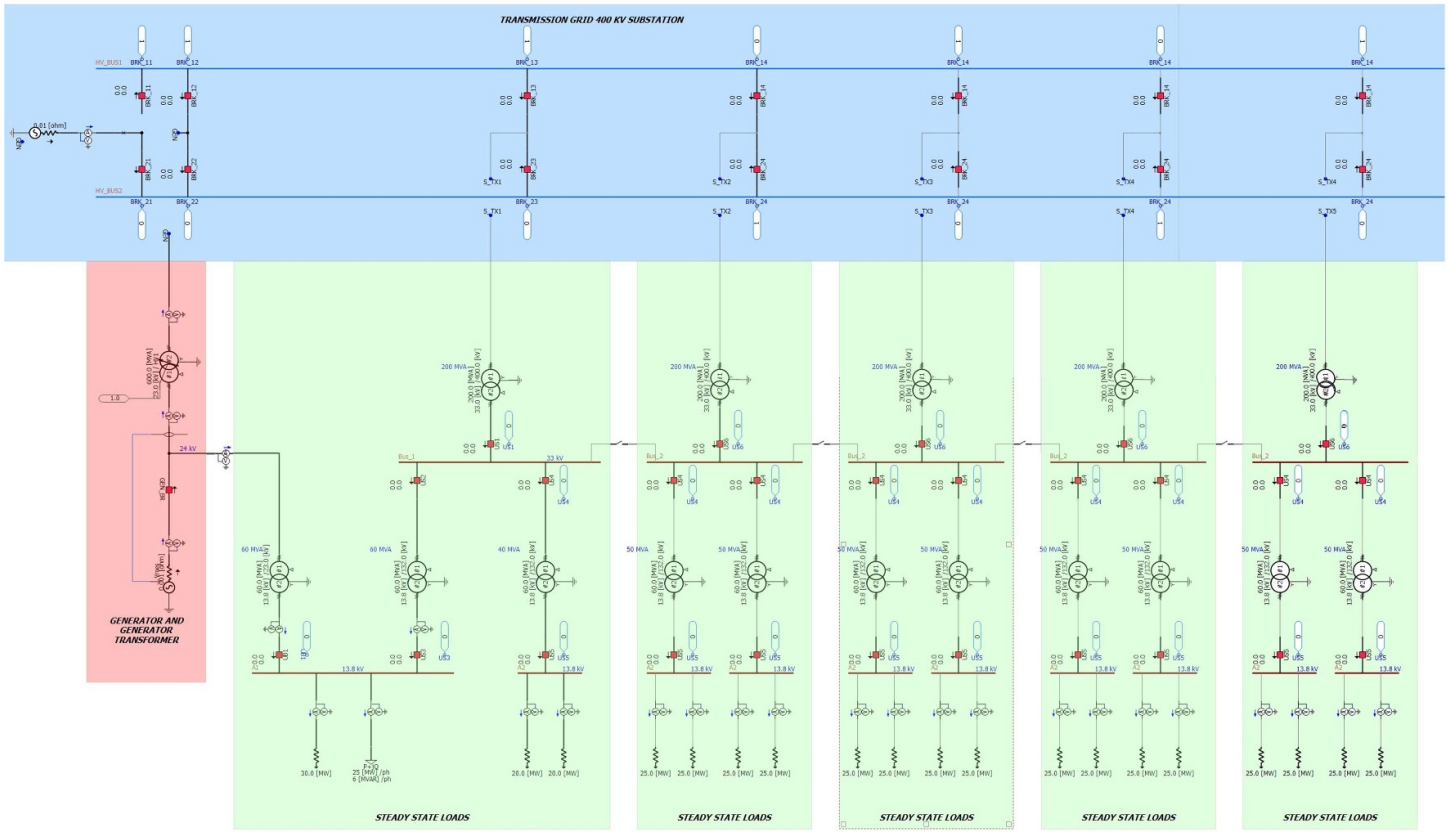

Figure 11. High level architecture of the ST-E1's power distribution system (steady-state and power generation).

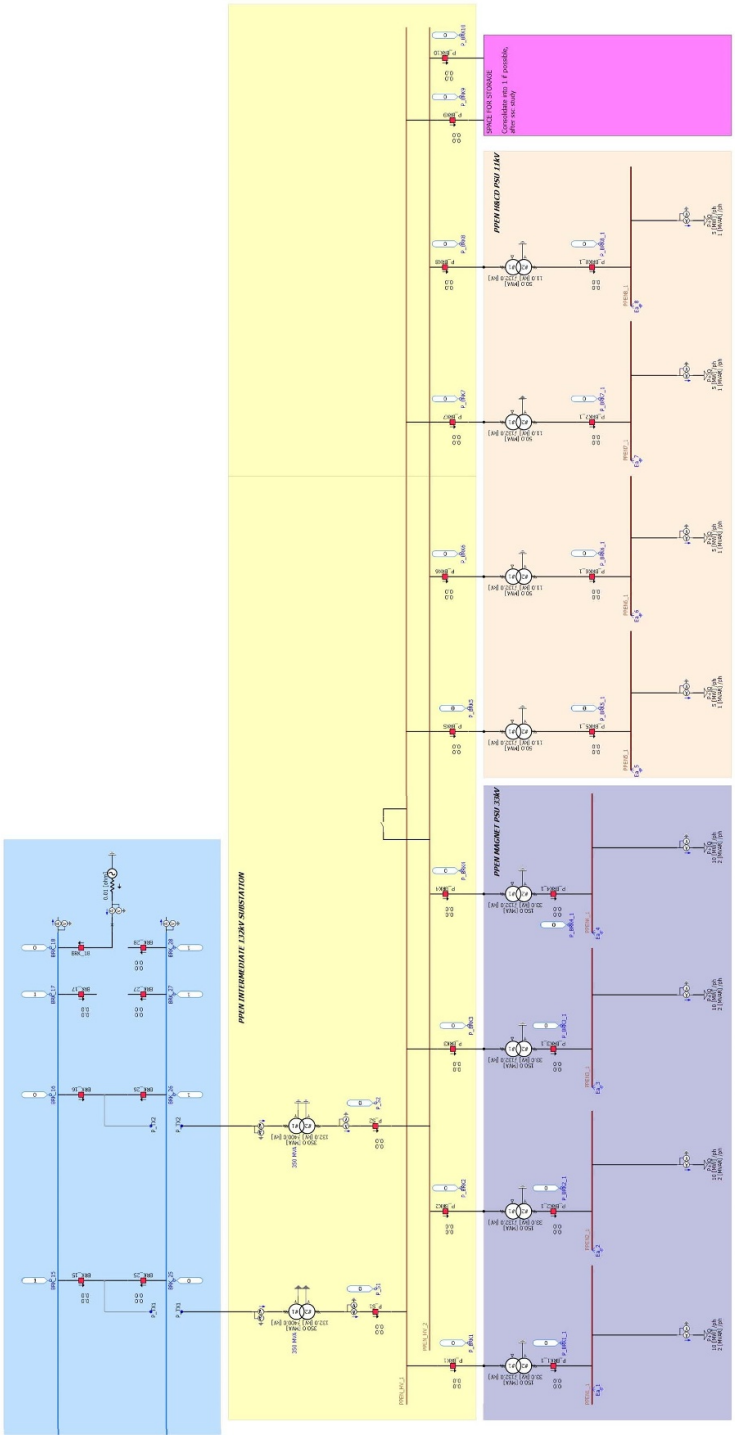

Figure 12. High level architecture of the ST-E1's power distribution system (pulsed power distribution).

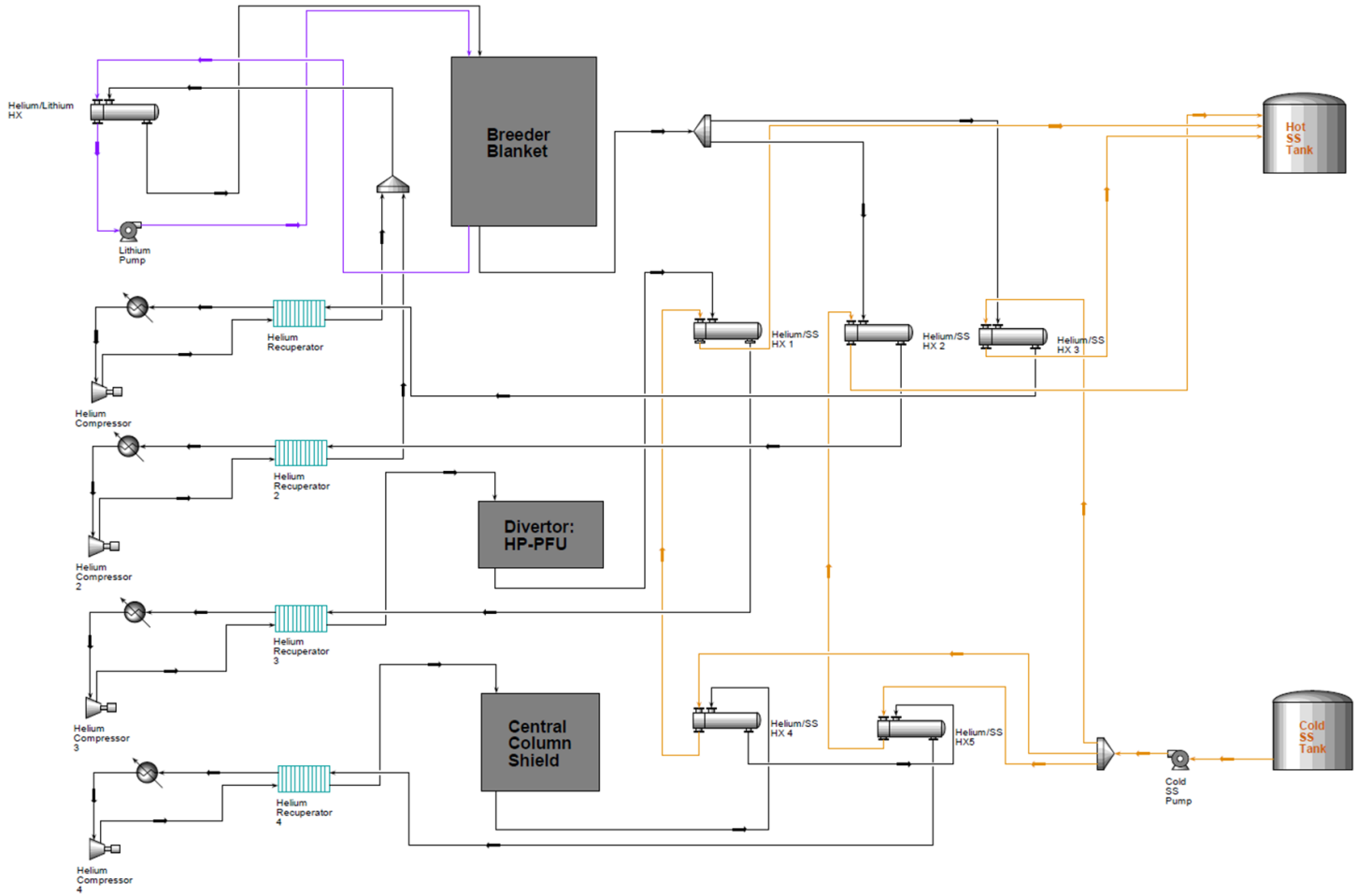

Figure 13. ST-E1's IHL thermal management process architecture modelled in Aspen HYSYS.

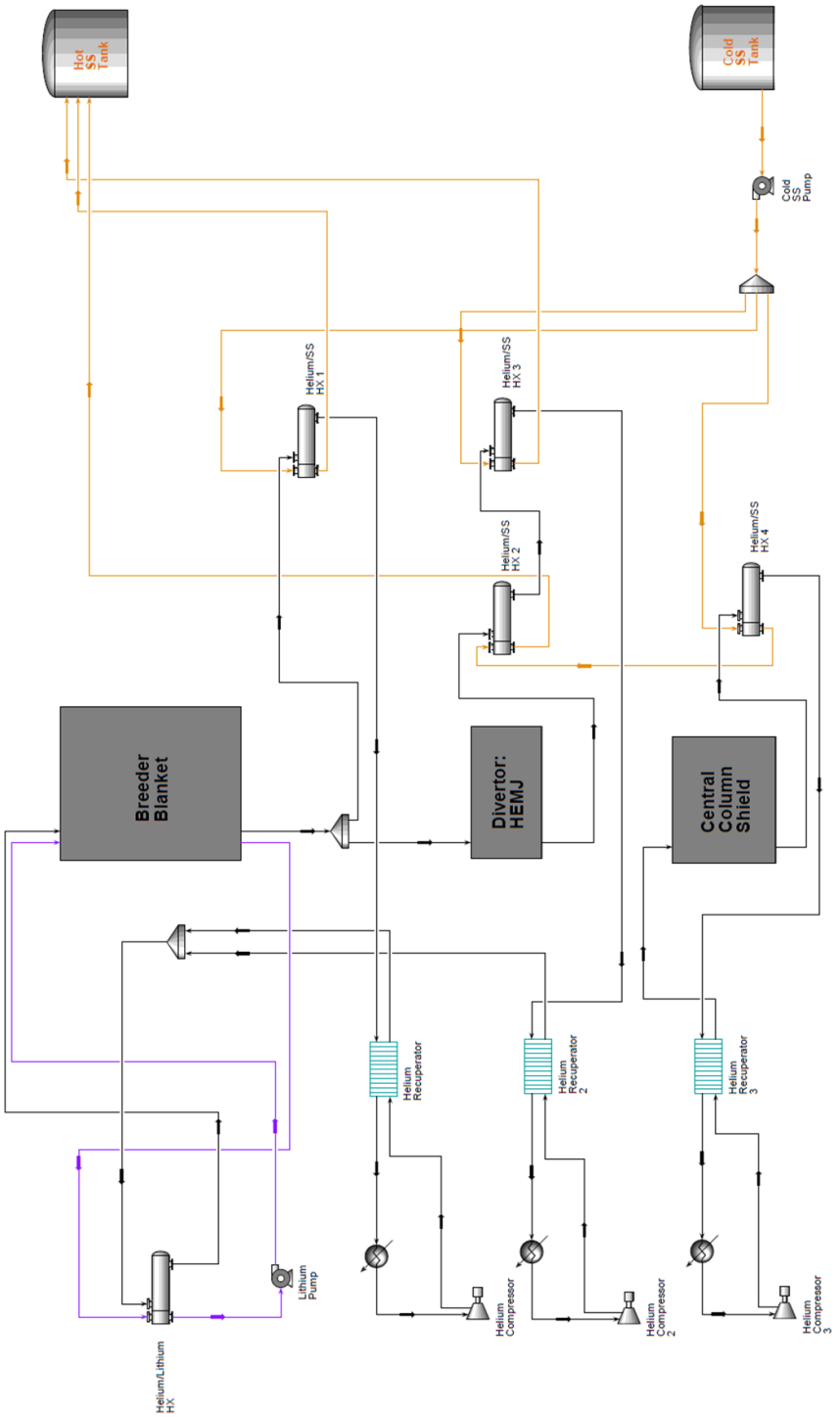

Figure 14. ST-E1's CHL thermal management process architecture modelled in Aspen HYSYS.

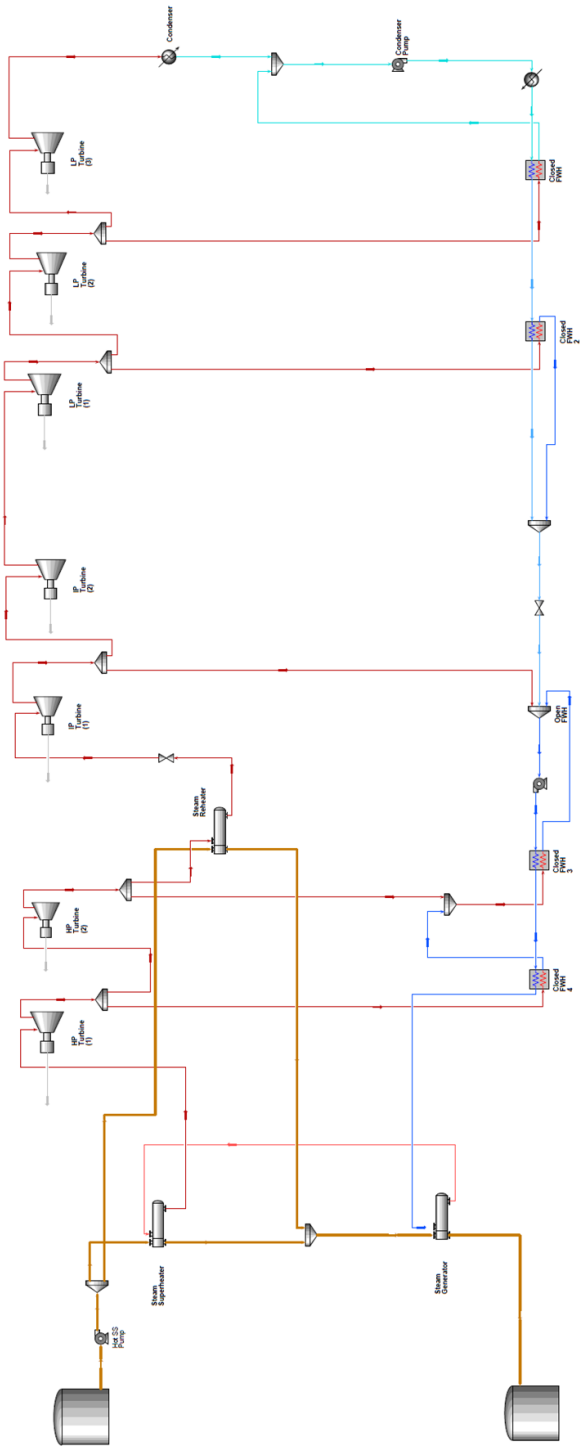

Figure 15. ST-E1's advanced supercritical steam process architecture modelled in Aspen HYSYS.

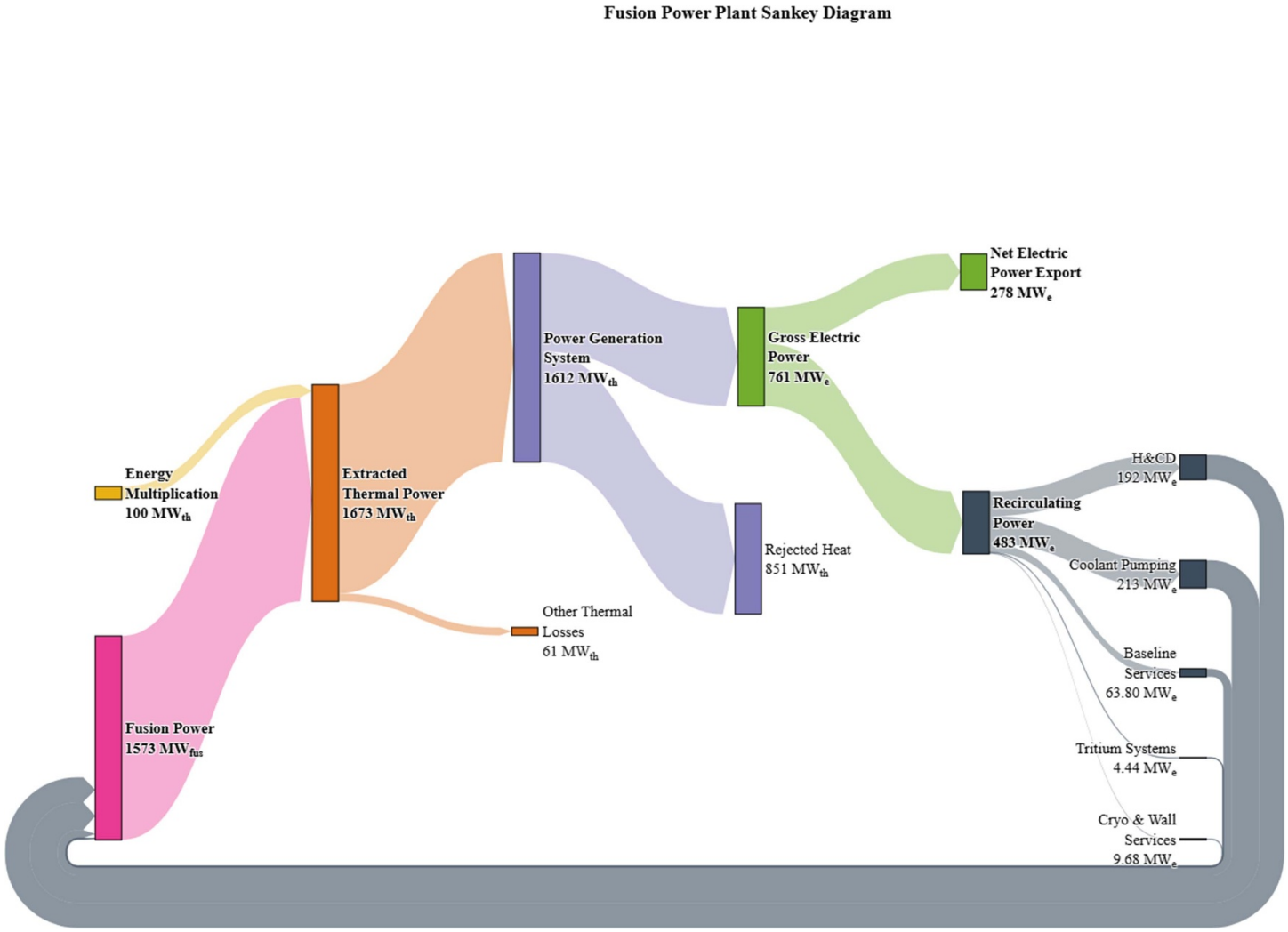

Figure 16. ST-E1 plant steady-state energy flow diagram (case 1).

5. Conclusions

This work presents a detailed evaluation of thermal management and net-power performance for the ST-E1 fusion power plant, emphasising the importance of integrated design in achieving grid-relevant fusion power. The analysis shows that auxiliary loads, particularly helium compression, dominate the recirculating power budget, making pressure-drop minimisation and pumping efficiency critical to plant viability. Pumping power emerges as a major constraint, and alternative coolant strategies, such as self-cooled breeder blankets or alternative coolants, offer potential to reduce parasitic losses and improve overall efficiency.

Achieving the pilot-phase target of 300–500 MWe requires extended flattop durations, driven by fixed energy penalties during ramp-up and ramp-down. While this underscores the need for plasma stability, improvements in thermal integration and system architecture can help relax these constraints. Structural material temperature limits further restrict coolant operating windows, influencing flowrates and pressure drops, which directly affect pumping power and thermal efficiency. These interdependencies highlight the need for careful coordination between material selection and thermal system design.

Thermal storage plays a pivotal role in smoothing power delivery and maintaining cycle stability. Current molten-salt systems provide operational flexibility but cap the maximum cycle temperature, limiting thermal-to-electric conversion efficiency. Exploring alternative storage media with higher operating temperatures could unlock significant gains in net power by enabling more effective heat recovery and reducing thermal losses.

In the longer term, stabilised reactor operation could enable direct coupling of primary heat sources to the power cycle, eliminating intermediate thermal buffers and improving efficiency. However, this approach introduces challenges related to thermal transients and contamination control, which require advanced integration strategies. Taken together, the ST-E1 concept demonstrates a credible pathway towards commercially relevant fusion power, provided that thermal management, pressure control, and system-level architecture are optimised to balance efficiency, reliability, and operational flexibility.

Acknowledgments

This work was undertaken as part of the US Department of Energy Milestone-based Fusion Development Program.

Funding

Tokamak Energy acknowledges U.S. Federal support for this work under TIA DE-SC0024889.

ORCID iDs

Mohamed Khalid Elsharif Mohamed 0009-0008-8892-0827
Alasdair Burchill 0009-0003-2910-8867
Liviu Maatescu 0009-0008-5391-6078
Emre Yildirim 0000-0002-1903-1857
Jonathan Naish 0009-0005-6763-490X
Matthew Robinson 0000-0003-0709-1219
Vandeep Godhani 0009-0001-0308-6298
Samara Levine 0000-0002-9562-104X
Chris Wilson 0009-0007-8860-3867
Robin Kamenicky 0000-0002-6292-2313
Abhishek Kumar 0000-0002-6026-5727

References

[1] Willis J. *et al* 2026 Tokamak Energy's pre-concept design for a fusion power plant: an overview of ST-E1 *Nucl. Fusion* **66** 086001
[2] Maartensson E.N.J. *et al* (the ST-E1 Team) 2026 Integrated physics and magnet design for the ST-E1 fusion power plant *Nucl. Fusion* **66** 086007
[3] Segal D., Cerfon A. and Freidberg J. 2021 Steady state versus pulsed tokamak reactors *Nucl. Fusion* **61** 045001
[4] Gaio E. *et al* 2022 Status and challenges for the concept design development of the EU DEMO plant electrical system *Fusion Eng. Des.* **177** 113052
[5] Wang Z. *et al* 2025 Fuel recycling and impurity characteristics in long-pulse H-mode plasmas with full metal and dynamically coated walls on EAST *Nucl. Fusion* **65** 104001
[6] Morris J. and Kovari M. 2017 Time-dependent power requirements for pulsed fusion reactors in systems codes *Fusion Eng. Des.* **124** 1203–6
[7] McNamara S.A.M. *et al* 2026 Physics basis for the reference flat-top plasma scenario in the ST-E1 fusion power plant *Nucl. Fusion* **66** 086008
[8] PSCAD (available at: www.pscad.com/)
[9] Neumeyer C. *et al* 2013 ITER power supply innovations and advances *2013 IEEE 25th Symp. on Fusion Engineering (SOFE)* (*San Francisco, CA, USA, 10–14 June 2013*) (IEEE) pp 1–8
[10] Minucci S., Panella S., Ciattaglia S., Falvo M.C. and Lampasi A. 2020 Electrical loads and power systems for the DEMO nuclear fusion project *Energies* **13** 2269
[11] Beach F. 1993 *Modern Power Station Practice: Incorporating Modern Power System Practice* (Pergamon)
[12] Kiank H. and Fruth W. 2011 *Planning Guide for Power Distribution Plants : Design, Implementation and Operation of Industrial Networks* (Wiley)
[13] IEEE 1994 *141-1993 - IEEE Recommended Practice for Electric Power Distribution for Industrial Plants (Color Book® series)* (IEEE) pp 1–768
[14] Ferro A. *et al* 2024 Overview on the applicability of the ITER/NPP-like technologies to the DEMO plant electrical system and promising alternatives *IEEE Trans. Plasma Sci.* **52** 3970–7
[15] Asuar O. *et al* 2003 ITER hot cell *Fusion Eng. Des.* **69** 153–6
[16] Tao J., Benfatto I., Goff J.K., Mankani A., Milani F., Song I., Tan H. and Thomsen J. 2011 ITER coil power supply and

distribution system *2011 IEEE/NPSS 24th Symp. on Fusion Engineering* (*Chicago, IL, USA*, *26–30 June 2011*) (IEEE) pp 1–8
[17] Lampasi A., Zito P., Starace F., Costa P., Maffia G., Minucci S., Gaio E., Toigo V., Zanotto L. and Ciattaglia S. 2017 The DTT device: power supplies and electrical distribution system *Fusion Eng. Des.* **122** 356–64
[18] Lampasi A. and Minucci S. 2017 Survey of electric power supplies used in nuclear fusion experiments *2017 IEEE Int. Conf. on Environment and Electrical Engineering and 2017 IEEE Industrial and Commercial Power Systems Europe (EEEIC/I&CPS Europe)* (*Milan, Italy*, *06–09 June 2017*) (IEEE) pp 1–6
[19] Shirai H., Takahashi K. and Di Pietro E. 2024 Recent progress of JT-60SA project toward plasma operation *Nucl. Fusion* **3** 112008
[20] Tran M. *et al* 2022 Status and future development of heating and current drive for the EU DEMO *Fusion Eng. Des.* **180** 113159
[21] Braunmueller F. *et al* 2024 Results on the 1 MW CW 170 GHz gyrotron TH1509UA for ITER and DTT at the FALCON test stand *EPJ Web Conf.* 313 04005
[22] Thumm M. 2025 State-of-the-art of high-power gyro-devices: 2025 update of experimental results *J. Infrared Millim. Terahertz Waves* **46** 35
[23] Jelonnek J. *et al* 2017 Design considerations for future DEMO gyrotrons: a review on related gyrotron activities within EUROfusion *Fusion Eng. Des.* **123** 241–6
[24] Smith K.S. and Mieee C. JET fusion experiment 36 kV enhancement studies *Technical Report*
[25] Ciattaglia S., Falvo M.C., Lampasi A. and Cosimi M.P. 2020 Energy analysis for the connection of the nuclear reactor DEMO to the european electrical grid *Energies* **13** 2157
[26] Zinkle S. and Ghoniem N. 2000 Operating temperature windows for fusion reactor structural materials *Fusion Eng. Des.* **51-52** 55–71
[27] Gietl H., Koyanagi T., Hu X., Fukuda M., Hasegawa A. and Katoh Y. 2022 Neutron irradiation-enhanced grain growth in tungsten and tungsten alloys *J. Alloys Compd.* **901** 163419
[28] Nogami S., Terentyev D., Zinovev A., Yin C., Rieth M., Pintsuk G. and Hasegawa A. 2021 Neutron irradiation tolerance of potassium-doped and rhenium-alloyed tungsten *J. Nucl. Mater.* **553** 153009
[29] Romano P.K., Horelik N.E., Herman B.R., Nelson A.G., Forget B. and Smith K. 2015 OpenMC: a state-of-the-art Monte Carlo code for research and development *Ann. Nucl. Energy* **82** 90–97
[30] Yildirim E. *et al* 2026 Tritium production and processing systems for ST-E1 *Nucl. Fusion* **66** 086004
[31] Ruck S., Kaiser B. and Arbeiter F. 2017 Thermal performance augmentation by rib-arrays for helium-gas cooled first wall applications *Fusion Eng. Des.* **124** 306–10
[32] Kirillov I.R., Reed C.B., Barleon L. and Miyazaki K. 1995 Present understanding of MHD and heat transfer phenomena for liquid metal blankets *Fusion Eng. Des.* **27** 553–69
[33] Hunt J.C.R. 1965 Magnetohydrodynamic flow in rectangular ducts *J. Fluid Mech.* **21** 577–90
[34] Yoda M. and Abdel-Khalik S.I. 2017 Overview of thermal hydraulics of helium-cooled solid divertors *Fusion Sci. Technol.* **72** 1–9
[35] Lee D., Lanahan M., Grohmann J., Abdel-Khalik S., Blanchard J. and Yoda M. 2024 Estimation of the thermal-fluids and thermal-structural performance of helium-cooled modular finger-type divertors *Fusion Eng. Des.* **200** 114217
[36] Robinson M. *et al* 2026 Power and particle exhaust in the ST-E1 fusion power plant *Nucl. Fusion* **66** 086011
[37] Rajput M. *et al* 2025 Performance characteristics and waste implications of WC materials used as neutron shielding materials in fusion *Int. J. Refract. Met. Hard Mater.* **132** 107280
[38] Chandrasekhar K., Wilson C.L., Levine S.M., Irukuvarghula S., Naish J.D., Godhani V.B., Márquez A.A. and Loughlin M.J. 2026 Nuclear technology considerations and neutronics for the ST-E1 fusion power plant *Nucl. Fusion* **66** 086003
[39] Suraparaju S.K., Samykano M., Namasivayam S., Kadirgama K. and Ramasamy D. 2024 Thermal stability and performance evaluation of Hitec Molten salt for high-temperature energy storage applications *E3S Web Conf.* 488 (EDP Sciences)
[40] Prieto C., Tagle-Salazar P.D., Patiño D., Schallenberg-Rodriguez J., Lyons P. and Cabeza L.F. 2024 Use of molten salts tanks for seasonal thermal energy storage for high penetration of renewable energies in the grid *J. Energy Storage* **86** 111203
[41] Steinbrecher J., Hanke A., Braun M., Bauer T. and Bonk A. 2023 Stabilization of solar salt at 650 °C–thermodynamics and practical implications for thermal energy storage systems *Sol. Energy Mater. Sol. Cells* **258** 112411
[42] Russo V., Napoli G., Rovense F., Di Ascenzi P., Giorgi G., Mongibello L., Cancro C., Ciniglio G. and Gaggioli W. 2025 Investigations on solidification and melting processes of the solar salt mixture in evacuated and non-evacuated receiver tubes *Energies* **18** 4492
[43] Aspen HYSYS® (available at: www.aspentech.com/en/products/engineering/aspen-hysys)
[44] Aspen Exchanger Design & Rating (EDR)® (available at: www.aspentech.com/en/products/engineering/aspen-exchanger-design-and-rating)
[45] Muto Y., Ishiyama S., Fukuyama Y., Okumoto J., Kishibe T. and Yamada S. 2000 Design study of helium turbine for the 300MW HTGR-GT power plant *Volume 2: Coal, Biomass and Alternative Fuels; Combustion and Fuels; Oil and Gas Applications; Cycle Innovations* (American Society of Mechanical Engineers)
[46] Malik A., Zheng Q. and Lin A. 2019 The design and performance analysis of highly loaded compressor of closed Brayton cycle HTGR power plant with helium xenon gas mixture as working fluid *Prog. Nucl. Energy* **117** 11
[47] Tian Z., Jiang B., Malik A. and Zheng Q. 2019 Axial helium compressor for high-temperature gas-cooled reactor: a review *Ann. Nucl. Energy* **130** 54–68
[48] Rein J., Hvasta M., Nollet W. and Anderson M. 2019 Enhancement of EM pump performance through modeling and testing *Technical Report*
[49] Arp V.D., McCarty R.D. and Friend D.G. 1998 Thermophysical properties of helium-4 from 0.8 to 1500 K with pressures to 2000 MPa (National Institute of Standards and Technology (NIST)) *Technical Report* (available at: https://nvlpubs.nist.gov/nistpubs/Legacy/TN/nbstechnicalnote1334.pdf)
[50] Davison H.W. 1968 Compilation of thermophysical properties of liquid lithium (NASA) *Technical Report*
[51] Zavoico A. 2001 Solar power tower design basis document, revision 0 Sandia National Laboratories (SNL) *Technical Report* Albuquerque, NM, and Livermore, CA (United States)
[52] Chase M.W. 1998 NIST-JANAF themochemical tables, monograph 9 *J. Phys. Chem. Ref. Data* **9** 1–1951 (available at: www.nist.gov/srd/journal-physical-and-chemical-reference-data-monographs-or-supplements)
[53] Bauer T., Odenthal C. and Bonk A. 2021 Molten salt storage for power generation *Chem. Ing. Tech.* **93** 534–46